Report no. NA-06/19

Finite Element Methods for Deterministic Simulation of Polymeric Fluids

David Knezevic

In this work we consider a finite element approach to solving the coupled Navier–Stokes (NS) and Fokker–Planck (FP) multiscale model that describes the dynamics of dilute polymeric fluids. Deterministic approaches such as ours have not received much attention in the literature because they present a formidable computational challenge due to the fact that the analytical solution of the Fokker–Planck equation may be a function of a large number of independent variables. For instance, to simulate a non-homogeneous flow one must solve the coupled NS–FP system in which (for a 3-dimensional flow, using the dumbbell model for polymers) the Fokker–Planck equation is posed in a 6-dimensional domain. In this work we seek to demonstrate the feasibility of our deterministic approach. We begin by discussing the physical and mathematical foundations of the NS–FP model. We then present a literature review of relevant developments in computational rheology and develop our deterministic finite element based approach in detail. Numerical results demonstrating the efficacy of our approach are then given, including some novel results for the simulation of a fully 3-dimensional flow. We utilise parallel computation in performing the larger-scale computations.

Key words and phrases: Polymer fluid dynamics, FENE dumbbell, finite element methods, multiscale modelling, parallel computing

Oxford University Computing Laboratory
Numerical Analysis Group
Wolfson Building
Parks Road
Oxford, England OX1 3QD

October, 2006

1 Introduction

1.1 Overview of polymer fluid dynamics

The study of the dynamics of polymeric fluids is a well-developed field that has been a focus of research for over 70 years. In part, interest in this field has been driven by the industrial and commercial applications of polymeric fluids. As well as this, though, polymer fluid dynamics has been increasingly attracting attention from the mathematics and numerical analysis communities due to the unique set of challenges this field presents. Specifically, polymer fluid dynamics is fundamentally "multiscale" in nature, in that in order to faithfully model the complicated rheological properties that these fluids exhibit there must be a coupling of the dynamics of microscopic polymer molecules with the macroscopic behaviour of the bulk flow. In this work we carefully detail the physics underlying the mathematical models we consider, while keeping an eye on considerations of interest to practitioners. However, our primary interest is to attempt to push the boundaries of mathematical and computational techniques in multiscale modelling as applied to polymer fluid dynamics.

With the inherent complexity of polymeric fluids and the resulting analytic intractability of many of the mathematical models in this area, computational approaches are playing an ever increasing role. In this work we propose a finite element methodology for the numerical simulation of dilute polymeric fluids. We defer discussion of this methodology until Section 2, however, as we first present an overview of the theory underpinning polymer fluid dynamics. We begin with a brief discussion of Newtonian fluids in Section 1.2, and then in Section 1.3 we introduce the "coarse-grained" mechanical models which are designed to capture the properties of polymer molecules which have the most significant effect on a fluid's rheological properties. We conclude this section by deriving the Fokker–Planck (FP) equation which describes the evolution of the probability density function for the configuration of polymers in a fluid. The FP equation governs the behaviour of polymer molecules on the microscopic scale, and is coupled with the Navier–Stokes (NS) equations which, as for Newtonian fluids, models the macroscopic flow. This is the coupling across scales that is inherent in polymer fluid dynamics.

1.2 Newtonian fluids

The success of classical fluid dynamics in accurately describing the properties of a wide range of fluids (typically with low molecular weight) using macroscopic continuum models is well established. We begin with a very brief review of some principles of classical fluid dynamics (following the presentation in Batchelor [3]) as this will be useful in elucidating important ideas in the theory of polymeric fluids. In the case of Newtonian fluids it has been experimentally established that in a shear flow, i.e. $u_x = u_x(y)$ where u_x is the x-component of the velocity field $\underset{\sim}{u}$, we can relate fluid stress to shear rate by

"Newton's law of viscosity":

$$\sigma_{yx} = \eta_s \frac{du_x}{dy}, \tag{1.1}$$

where σ_{yx} denotes the force per unit area acting in the x-direction, on a surface normal to the y-direction. That is, stress is proportional to shear rate and the viscosity, η_s, is the constant of proportionality. This relationship can be generalised to a tensor equation relating the stress tensor, $\underset{\approx}{\sigma}$, and the strain tensor $\underset{\sim}{\nabla}\underset{\sim}{u} + (\underset{\sim}{\nabla}\underset{\sim}{u})^T$, as follows:

$$\underset{\approx}{\sigma} = -p\underset{\approx}{I} + \eta_s(\underset{\sim}{\nabla}\underset{\sim}{u} + (\underset{\sim}{\nabla}\underset{\sim}{u})^T).$$

This equation provides a relationship between the stress and strain (in this case, a simple linear equation) and is known as a *constitutive equation*.

Combining the Newtonian constitutive equation with the equations of conservation of mass:

$$\underset{\sim}{\nabla} \cdot \underset{\sim}{u} = 0,$$

and momentum:

$$\rho\left(\frac{\partial \underset{\sim}{u}}{\partial t} + \underset{\sim}{u} \cdot \underset{\sim}{\nabla}\underset{\sim}{u}\right) = \underset{\sim}{\nabla} \cdot \underset{\approx}{\sigma},$$

where ρ is the fluid density, gives rise to the Navier–Stokes equations for an incompressible, viscous, isothermal fluid:

$$\begin{aligned} \rho\left(\frac{\partial \underset{\sim}{u}}{\partial t} + \underset{\sim}{u} \cdot \underset{\sim}{\nabla}\underset{\sim}{u}\right) - \eta_s \Delta \underset{\sim}{u} + \underset{\sim}{\nabla} p &= 0, \\ \underset{\sim}{\nabla} \cdot \underset{\sim}{u} &= 0. \end{aligned}$$

These equations (which involve only macroscopic quantities) form the cornerstone of classical fluid dynamics. Modelling polymeric fluids, however, requires a more complicated constitutive equation than "Newton's law of viscosity". In the next section we discuss modelling of polymeric fluids on the microscopic (i.e. molecular) scale, which is generally the starting point for deriving a constitutive equation.

1.3 Polymeric fluids

Polymer molecules (often referred to as *macromolecules*) consist of long chains of repeated basic structural units, or *monomers*. Due to the properties of these macromolecules, polymeric fluids behave very differently to Newtonian fluids and are described as *viscoelastic* to emphasise the fact that they have both viscous and elastic properties (elastic in the sense that the fluid has memory of past deformations). This viscoelasticity gives rise to an exotic range of phenomena, such as shear-thinning, rod-climbing, the "tubeless siphon", and elastic recoil [6].

The goal of polymer fluid dynamics is to derive and analyse mathematical models that capture this complex viscoelastic behaviour. As indicated earlier, this requires the development of a constitutive equation for the fluid. The traditional approach was to derive a constitutive equation (typically an algebraic or differential equation) involving

only macroscopic quantities that relates the viscoelastic stress to the deformation history [6]. Such macroscopic constitutive equations can be based on purely macroscopic considerations, but more often they are derived from kinetic theory as kinetic–theory–based analysis enables greater modelling flexibility and has been shown to lead to more realistic models. However, except in the simplest cases, such as the Hookean dumbbell model (see Section 1.4), deriving a purely macroscopic constitutive equation from a kinetic theory model requires closure approximations which compromise the accuracy of the model [21].

The traditional focus on closure approximations is understandable as it requires far less work to compute the solution of a model that involves only macroscopic variables, and indeed in many cases (particularly for simple flows) these macroscopic models can be solved analytically. However, with the explosion of available computational power it has become possible and desirable to compute with the more accurate "micro-macro" multiscale models directly (this approach gained popularity in the early 1990s, see Section 2). Our focus is on multiscale models and as a result we will give no more attention to purely macroscopic models. It is worth stating, however, that the macroscopic approach is still an essential part of theoretical and computational rheology and the distinct advantages of computational efficiency and mathematical tractability that macroscopic models enjoy will ensure that they will remain significant for the foreseeable future.

1.4 Models of polymer chains

In order to derive kinetic–theory–based equations for the behaviour of polymeric fluids we require a simple representation of a single polymer molecule. A mechanical model that would faithfully capture the microscopic properties of an actual polymer would be extremely complicated, with a very high number of degrees of freedom. To make mathematical analysis tractable, a variety of polymer models have been proposed over the last 50 years (see Chapter 10 of Bird *et. al.* [7] for a discussion of the most important examples). Two widely used models are the *Kramers chain* [23] and the *Rouse-Zimm chain* [31,35]. These both model the polymer as a chain of beads. For the Kramers chain, the beads are connected by rigid, massless rods whereas in the case of the Rouse-Zimm chain springs (with force law $\underset{\sim}{F}$) are used as connectors.

However, such chain models can be prohibitively expensive to use in numerical simulations because they typically have a large number of degrees of freedom (e.g. $O(10)$ or $O(10^2)$). As a result, much attention has been focused on the simplest in the hierarchy of polymer models, the dumbbell model. This model consists of just two masses connected by a spring (or sometimes a rigid rod, although we will only discuss the spring case here). A dumbell is fully specified if we know the position of its centre of mass, $\underset{\approx}{x}$ and its end-to-end vector, $\underset{\sim}{q}$. We refer to the domain of $\underset{\approx}{x}$ as *physical space* and the domain of $\underset{\sim}{q}$ as *configuration space*. Figure 1 shows a schematic dumbell and the two quantities $\underset{\approx}{x}$ and $\underset{\sim}{q}$ are labelled. Despite the simplicity of the dumbbell model, it can be very useful in simulating the behaviour of polymeric fluids. This is because a dumbbell can be stretched and oriented by a flow, and these two actions largely determine the rheological properties of a polymeric fluid in many cases.

The dumbbell model depends on the choice of a force law for the spring. The two most common choices are Hookean springs,

$$\underset{\sim}{F}(\underset{\sim}{q}) = H\underset{\sim}{q}, \tag{1.3}$$

and Finitely Extensible Non-linear Elastic (FENE) springs [34],

$$\underset{\sim}{F}(\underset{\sim}{q}) = \frac{H\underset{\sim}{q}}{1 - |\underset{\sim}{q}|^2/Q_{max}^2}, \tag{1.4}$$

where $\underset{\sim}{F}$ is the spring force, $\underset{\sim}{q}$ is the end-to-end vector of a single spring and H is the spring constant.

The case of a Hookean spring has been studied extensively as it enables a range of analytical results to be obtained. In particular, it can be shown that the well-known Oldroyd-B model for dilute polymeric fluids (originally derived from continuum mechanics considerations [29]) is equivalent to the Hookean dumbbell micro-macro model [1]. However, due to physically unrealistic ability of Hookean springs to be infinitely stretched, this model can break down in certain cases such as strong extensional flows.

In such cases, one can use the FENE spring model, which has a maximum extension of Q_{max}. The FENE dumbbell model is more realistic than the Hookean model, but on using the non-linear FENE force law we sacrifice any hope of deriving analytic results for non-equilibrium flows. Hence FENE springs necessitate a computational approach.

Our goal is to develop and analyse efficient finite-element based numerical methods to solve the system of equations that arise from the multiscale modelling of dilute polymeric fluids. This presents a significant challenge even when using the dumbbell model because (as discussed in Section 1.5) for the general case of a 3-dimensional flow, we must solve a system in which the NS and FP equations are coupled, and in which the FP equation is posed in 6-dimensions (since individual dumbells have 6 degrees-of-freedom, 3 for $\underset{\sim}{x}$ and 3 for $\underset{\sim}{q}$). If our methodology can be successfully applied to the equations arising from the dumbbell model then a goal of future work would be to extend this to the bead-spring chain case.

1.5 The coupled Navier–Stokes Fokker–Planck model

We are interested in modelling a dilute solution of polymer chains suspended in a Newtonian solvent in which it is assumed that individual polymer chains do not interact with one another. Suppose the fluid is confined to a physical domain Ω, assumed to be an open set in $\mathbb{R}^d, d = 2, 3$, and that we impose some appropriate boundary conditions on $\partial\Omega$, e.g. the no-slip condition or a periodic boundary condition. The conservation equations are the same as for the Newtonian case, but the presence of polymer molecules in the fluid contribute a *polymeric extra-stress*, represented by the tensor $\underset{\approx}{\tau}$. That is, the total stress tensor $\underset{\approx}{\sigma}$ is given by

$$\underset{\approx}{\sigma} = -p\underset{\approx}{I} + \eta_s(\underset{\sim}{\nabla}\underset{\sim}{u} + (\underset{\sim}{\nabla}\underset{\sim}{u})^T) + \underset{\approx}{\tau}. \tag{1.5}$$

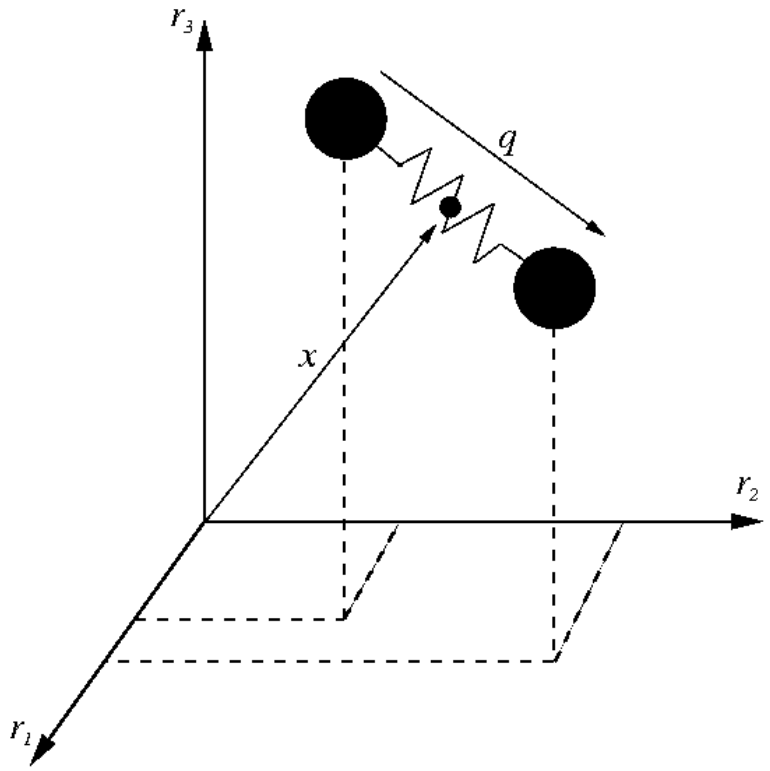

Figure 1: The dumbbell model consists of two beads joined by a spring. The state of a dumbbell is defined by the position of its centre of mass, $\underset{\sim}{x}$, and its end-to-end vector, $\underset{\sim}{q}$.

Combining (1.5) with the conservation of mass and momentum equations, we obtain the Navier–Stokes equations with $\underset{\approx}{\tau}$ arising as a source term. Thus our model problem takes the following form:

Find $\underset{\sim}{u} : (\underset{\sim}{x}, t) \in \Omega \times \mathbb{R} \to \underset{\sim}{u}(\underset{\sim}{x}, t) \in \mathbb{R}^d$ and $p : (\underset{\sim}{x}, t) \in \Omega \times \mathbb{R} \to p(\underset{\sim}{x}, t) \in \mathbb{R}$ such that

$$\rho\left(\frac{\partial \underset{\sim}{u}}{\partial t} + \underset{\sim}{u} \cdot \underset{\sim}{\nabla}\underset{\sim}{u}\right) - \eta_s \Delta \underset{\sim}{u} + \underset{\sim}{\nabla} p = \underset{\sim}{\nabla} \cdot \underset{\approx}{\tau} \quad \text{in } \Omega \times (0, T], \tag{1.6a}$$

$$\underset{\sim}{\nabla} \cdot \underset{\sim}{u} = 0 \quad \text{in } \Omega \times (0, T], \tag{1.6b}$$

$$\underset{\sim}{u}(\underset{\sim}{x}, 0) = \underset{\sim}{u}_0(\underset{\sim}{x}) \quad \forall \underset{\sim}{x} \in \Omega, \tag{1.6c}$$

where η_s is the solvent viscosity. We complete the system with appropriate boundary conditions on $\partial\Omega$.

In general, the rheological properties of a polymeric fluid are determined by the statistical distribution of the configuration (i.e. orientation and degree of stretching) of individual polymer molecules within the fluid [20]. Measurable macroscopic quantities, such as the stress tensor $\underset{\approx}{\tau}$, are defined as statistical averages of some function of the configuration distribution. Therefore, our strategy is to first compute the configuration distribution, enabling us to determine $\underset{\approx}{\tau}$, and then we can solve Eq.(1.6a–1.6c). As discussed in Section 1.4, a hierarchy of mechanical models for polymer molecules have been

proposed. These models are useful not because they accurately capture the physical characteristics of actual polymer molecules (which are impressively complex structures) but rather because they enable us to model the microscopic behaviour of a polymeric fluid. In this work we utilise only the dumbbell model, and we propose a computational framework with which it is feasible to deterministically compute the dumbbell configuration distribution throughout Ω, which then enables us to solve the coupled NS–FP system.

1.5.1 The Fokker–Planck equation

We now derive the partial differential equation, known as the Fokker–Planck equation (or sometimes the diffusion equation), that quantitatively describes the statistical distribution of the configuration of polymer molecules throughout the physical domain Ω. In this derivation we closely follow the arguments presented in Bird *et. al.* [7], the Ph.D. thesis by Lozinski [25] and the paper by Barrett & Süli [2].

We begin by considering an isolated dumbbell immersed in a Newtonian solvent, with fluid velocity given by $\underset{\sim}{u}(\underset{\sim}{x},t)$. Denote by $\underset{\sim}{r}_1(t) \in \mathbb{R}^d$ and $\underset{\sim}{r}_2(t) \in \mathbb{R}^d$ the position vectors of the two dumbbell masses at time t. Then, referring to Figure 1, we define the centre of mass, $\underset{\sim}{x}(t)$, as

$$\underset{\sim}{x}(t) = \frac{1}{2}\left(\underset{\sim}{r}_1(t) + \underset{\sim}{r}_2(t)\right),$$

and the end-to-end vector, $\underset{\sim}{q}(t)$, as

$$\underset{\sim}{q}(t) = \underset{\sim}{r}_2(t) - \underset{\sim}{r}_1(t).$$

Hence we have $\underset{\sim}{x} \in \Omega$ and $\underset{\sim}{q}(t) \in D$, where D denotes *configuration space*. For the two dumbbell models of interest in this work, Hookean and FENE dumbbells, configuration space is $\mathbb{R}^d$ and $B(0, Q_{max})$ respectively, where $B(0,s)$ is the d-dimensional ball centered at the origin with radius s.

Considering an isolated dumbbell (in which, following [2], we neglect acceleration terms since the bead masses are small) Langevin's equation for each bead takes the form

$$\zeta\left(\dot{\underset{\sim}{r}}_1(t) - \underset{\sim}{u}(\underset{\sim}{r}_1(t),t)\right) = \underset{\sim}{B}_1(t) + \underset{\sim}{F}(\underset{\sim}{r}_2(t) - \underset{\sim}{r}_1(t)), \tag{1.7a}$$

$$\zeta\left(\dot{\underset{\sim}{r}}_2(t) - \underset{\sim}{u}(\underset{\sim}{r}_2(t),t)\right) = \underset{\sim}{B}_2(t) + \underset{\sim}{F}(\underset{\sim}{r}_1(t) - \underset{\sim}{r}_2(t)), \tag{1.7b}$$

where ζ is a friction coefficient and $\underset{\sim}{B}_i(t)$ is the Brownian force acting on bead i at time t, which is given by a d-component Wiener process. The spring force $\underset{\sim}{F} : D \subset \mathbb{R}^d \to \mathbb{R}^d$ is given by either the Hookean (1.3) or FENE (1.4) force law.

Let $f(\underset{\sim}{r}_1, \underset{\sim}{r}_2, \dot{\underset{\sim}{r}}_1, \dot{\underset{\sim}{r}}_2, t)$ denote the probability density function over *phase space* (i.e. $(\underset{\sim}{r}_1, \underset{\sim}{r}_2, \dot{\underset{\sim}{r}}_1, \dot{\underset{\sim}{r}}_2) \subset \mathbb{R}^{4d}$) such that $f(\underset{\sim}{r}_1, \underset{\sim}{r}_2, \dot{\underset{\sim}{r}}_1, \dot{\underset{\sim}{r}}_2, t)\mathrm{d}\underset{\sim}{r}_1\mathrm{d}\underset{\sim}{r}_2\mathrm{d}\dot{\underset{\sim}{r}}_1\mathrm{d}\dot{\underset{\sim}{r}}_2$ is the expected number of dumbells having bead positions and velocities inside the differential boxes $[\underset{\sim}{r}_i, \underset{\sim}{r}_i + \mathrm{d}\underset{\sim}{r}_\mathrm{i}]$ and $[\dot{\underset{\sim}{r}}_i, \dot{\underset{\sim}{r}}_i + \mathrm{d}\dot{\underset{\sim}{r}}_\mathrm{i}]$ at time t.

Define the velocity-space average $\langle\!\langle \cdot \rangle\!\rangle$ for a function A by

$$\langle\!\langle A \rangle\!\rangle(\underset{\sim}{r}_1, \underset{\sim}{r}_2, t) = \frac{1}{\psi^{12}(\underset{\sim}{r}_1, \underset{\sim}{r}_2, t)} \int_{\dot{r}_1 \dot{r}_2} A(\underset{\sim}{r}_1, \underset{\sim}{r}_2, \underset{\sim}{\dot{r}}_1, \underset{\sim}{\dot{r}}_2, t) f(\underset{\sim}{r}_1, \underset{\sim}{r}_2, \underset{\sim}{\dot{r}}_1, \underset{\sim}{\dot{r}}_2, t) \mathrm{d}\underset{\sim}{\dot{r}}_1 \mathrm{d}\underset{\sim}{\dot{r}}_2$$

where ψ^{12} is the marginal distribution of f:

$$\psi^{12}(\underset{\sim}{r}_1, \underset{\sim}{r}_2, t) = \int_{\dot{r}_1 \dot{r}_2} f(\underset{\sim}{r}_1, \underset{\sim}{r}_2, \underset{\sim}{\dot{r}}_1, \underset{\sim}{\dot{r}}_2, t) \mathrm{d}\underset{\sim}{\dot{r}}_1 \mathrm{d}\underset{\sim}{\dot{r}}_2.$$

From [7], we have that ψ^{12} satisfies the following "continuity equation",

$$\frac{\partial \psi^{12}}{\partial t} + \underset{\sim}{\nabla}_{r_1} \cdot (\langle\!\langle \underset{\sim}{\dot{r}}_1 \rangle\!\rangle \psi^{12}) + \underset{\sim}{\nabla}_{r_2} \cdot (\langle\!\langle \underset{\sim}{\dot{r}}_2 \rangle\!\rangle \psi^{12}) = 0. \tag{1.8}$$

We apply the velocity-space average $\langle\!\langle \cdot \rangle\!\rangle$ to (1.7a) and (1.7b) to obtain

$$\begin{aligned} \zeta \left(\langle\!\langle \underset{\sim}{\dot{r}}_1(t) \rangle\!\rangle - \underset{\sim}{u}(\underset{\sim}{r}_1(t), t) \right) &= \langle\!\langle \underset{\sim}{B}_1(t) \rangle\!\rangle + \underset{\sim}{F}(\underset{\sim}{r}_2(t) - \underset{\sim}{r}_1(t)), & (1.9a) \\ \zeta \left(\langle\!\langle \underset{\sim}{\dot{r}}_2(t) \rangle\!\rangle - \underset{\sim}{u}(\underset{\sim}{r}_2(t), t) \right) &= \langle\!\langle \underset{\sim}{B}_2(t) \rangle\!\rangle + \underset{\sim}{F}(\underset{\sim}{r}_1(t) - \underset{\sim}{r}_2(t)). & (1.9b) \end{aligned}$$

This brings us to an important point in the derivation. We make the standard assumption that the fluid velocity distribution is Maxwellian about the velocity at the centre of mass of the dumbbell. This assumption is referred to as "equilibrium in momentum space". Making this assumption leads to a simplified form of the velocity average of the Brownian force:

$$\langle\!\langle B_i(t) \rangle\!\rangle = -kT \nabla_{r_i} \ln \psi^{12} = -kT \frac{\nabla_{r_i} \psi^{12}}{\psi^{12}},$$

where k is Boltzmann's constant and T is the absolute temperature. Substituting this into equations (1.9a) and (1.9b) yields:

$$\langle\!\langle \underset{\sim}{\dot{r}}_1 \rangle\!\rangle \psi_{12} = -\frac{kT}{\zeta} \underset{\sim}{\nabla}_{r_1} \psi^{12} + \underset{\sim}{u}(\underset{\sim}{r}_1, t) \psi^{12} + \frac{1}{\zeta} \underset{\sim}{F}(\underset{\sim}{r}_2 - \underset{\sim}{r}_1) \psi^{12}, \tag{1.10a}$$

$$\langle\!\langle \underset{\sim}{\dot{r}}_2 \rangle\!\rangle \psi_{12} = -\frac{kT}{\zeta} \underset{\sim}{\nabla}_{r_2} \psi^{12} + \underset{\sim}{u}(\underset{\sim}{r}_2, t) \psi^{12} + \frac{1}{\zeta} \underset{\sim}{F}(\underset{\sim}{r}_1 - \underset{\sim}{r}_2) \psi^{12}. \tag{1.10b}$$

Combining Eqs. (1.10a) and (1.10b) with the continuity equation (1.8) gives us a Fokker–Planck equation for ψ^{12}:

$$\begin{aligned} \frac{\partial \psi^{12}}{\partial t} &+ \underset{\sim}{\nabla}_{r_1} \cdot \left[\underset{\sim}{u}(\underset{\sim}{r}_1, t) \psi^{12} + \frac{1}{\zeta} \underset{\sim}{F}(\underset{\sim}{r}_2 - \underset{\sim}{r}_1) \psi^{12} \right] \\ &+ \underset{\sim}{\nabla}_{r_2} \cdot \left[\underset{\sim}{u}(\underset{\sim}{r}_2, t) \psi^{12} + \frac{1}{\zeta} \underset{\sim}{F}(\underset{\sim}{r}_1 - \underset{\sim}{r}_2) \psi^{12} \right] \\ &= \frac{kT}{\zeta} \Delta_{r_1} \psi^{12} + \frac{kT}{\zeta} \Delta_{r_2} \psi^{12}. \end{aligned} \tag{1.11}$$

Next, let $\psi(\underset{\sim}{x},\underset{\sim}{q},t) = \psi^{12}(\underset{\sim}{x}-\underset{\sim}{q}/2,\underset{\sim}{x}+\underset{\sim}{q}/2,t)$. Substituting $\psi(\underset{\sim}{x},\underset{\sim}{q},t)$ into Eq.(1.11), we get:

$$\begin{aligned}\frac{\partial\psi}{\partial t} &+ \underset{\sim}{\nabla}_x\cdot\left(\frac{\underset{\sim}{u}(\underset{\sim}{x}-\underset{\sim}{q}/2)+\underset{\sim}{u}(\underset{\sim}{x}+\underset{\sim}{q}/2)}{2}\psi\right)\\ &+ \underset{\sim}{\nabla}_q\cdot\left(\left(\left[\underset{\sim}{u}(\underset{\sim}{x}+\underset{\sim}{q}/2,t)-\underset{\sim}{u}(\underset{\sim}{x}-\underset{\sim}{q}/2,t)\right]\frac{2}{\zeta}\underset{\sim}{F}(\underset{\sim}{q})\right)\psi\right)\\ &= \frac{kT}{2\zeta}\Delta_x\psi+\frac{2kT}{\zeta}\Delta_q\psi,\end{aligned}\tag{1.12}$$

where x and q subscripts indicate gradients in physical and configuration space respectively. To put this equation into its standard form we introduce the characteristic relaxation time, $\lambda=\zeta/4H$ and non-dimensionalise in configuration space by setting $\hat{\underset{\sim}{q}}=\underset{\sim}{q}/l_0$, where $l_0=\sqrt{kT/H}$ is the characteristic dumbbell length. Let us use the symbol $\hat{}$ to denote a function that has been non-dimensionalised with respect to the variable $\hat{\underset{\sim}{q}}$. The non-dimensional spring force laws are then given by:

$$\hat{\underset{\sim}{F}}(\hat{\underset{\sim}{q}})=\hat{\underset{\sim}{q}}\tag{1.13}$$

for Hookean springs and

$$\hat{\underset{\sim}{F}}(\hat{\underset{\sim}{q}})=\frac{\hat{\underset{\sim}{q}}}{1-|\hat{\underset{\sim}{q}}|^2/b},\tag{1.14}$$

for FENE springs, where $\hat{\underset{\sim}{q}}\in[0,\sqrt{b}]$ and $b=Q^2_{max}/l_0^2$ is a dimensionless parameter typically in the range $b\in[10,1000]$. Then $\underset{\sim}{F}(\underset{\sim}{q})=Hl_0\hat{\underset{\sim}{F}}(\hat{\underset{\sim}{q}})$. Similarly, $l_0^d\psi(\underset{\sim}{x},\underset{\sim}{q},t)=l_0^d\psi(\underset{\sim}{x},l_0\hat{\underset{\sim}{q}},t)=\hat{\psi}(\underset{\sim}{x},\hat{\underset{\sim}{q}},t)$, where the factor l_0^d is due to the fact that ψ represents the density of polymer molecules. Later we will normalise $\hat{\psi}$ so that it is a probability density function (pdf). Also, $\underset{\sim}{\nabla}_q=\frac{1}{l_0}\underset{\sim}{\nabla}_{\hat{q}}$ and $\Delta_q=\frac{1}{l_0^2}\Delta_{\hat{q}}$. Applying these transformations to Eq.(1.12), and cancelling $\frac{1}{l_0^d}$ (arising from non-dimensionalising ψ) from each term, we obtain:

$$\begin{aligned}\frac{\partial\hat{\psi}}{\partial t} &+ \frac{\underset{\sim}{u}(\underset{\sim}{x}-l_0\hat{\underset{\sim}{q}}/2)+\underset{\sim}{u}(\underset{\sim}{x}+l_0\hat{\underset{\sim}{q}}/2)}{2}\cdot\underset{\sim}{\nabla}_x\hat{\psi}\\ &+ \underset{\sim}{\nabla}_{\hat{q}}\cdot\left(\left(\frac{1}{l_0}\left[\underset{\sim}{u}(\underset{\sim}{x}+l_0\hat{\underset{\sim}{q}}/2,t)-\underset{\sim}{u}(\underset{\sim}{x}-l_0\hat{\underset{\sim}{q}}/2,t)\right]-\frac{1}{2\lambda}\hat{\underset{\sim}{F}}(\hat{\underset{\sim}{q}})\right)\hat{\psi}\right)\\ &= \frac{l_0^2}{8\lambda}\Delta_x\hat{\psi}+\frac{1}{2\lambda}\Delta_{\hat{q}}\hat{\psi}.\end{aligned}\tag{1.15}$$

The other term in Eq.(1.15) arising from $\underset{\sim}{\nabla}_x\cdot\left(\frac{\underset{\sim}{u}(\underset{\sim}{x}-\underset{\sim}{q}/2)+\underset{\sim}{u}(\underset{\sim}{x}+\underset{\sim}{q}/2)}{2}\psi\right)$ in Eq.(1.12) vanishes because of incompressibility. To simplify notation we henceforth drop the $\hat{}$ symbol, but the equations are understood to be non-dimensionalised with respect to configuration space.

In order to simplify Eq.(1.15) further we need to adopt the *local homogeneity assumption*, which states that $\underset{\sim}{u}$ and ψ are linear on the length scale of a dumbbell. Hence we can represent each of $\underset{\sim}{u}(\underset{\sim}{x} + l_0\underset{\sim}{q}/2)$ and $\underset{\sim}{u}(\underset{\sim}{x} - l_0\underset{\sim}{q}/2)$ using a Taylor series up to the linear term, to obtain:

$$\frac{\partial \psi}{\partial t} + (\underset{\sim}{u} \cdot \underset{\sim}{\nabla}_x)\psi + \underset{\sim}{\nabla}_q \cdot \left(\left(\underset{\approx}{\kappa}\underset{\sim}{q} - \frac{1}{2\lambda}\underset{\sim}{F}(\underset{\sim}{q}) \right) \psi \right) = \frac{l_0^2}{8\lambda}\Delta_x\psi + \frac{1}{2\lambda}\Delta_q\psi. \tag{1.16}$$

where $\underset{\approx}{\kappa} = \underset{\sim}{\nabla}_x \underset{\sim}{u}$ and $\mathrm{tr}(\underset{\approx}{\kappa}) = 0$ to ensure incompressibility. At this point it is worth noting that a significant amount of work in the literature has focused on so-called "homogeneous flows" in which $\underset{\approx}{\kappa}$ is constant throughout Ω (although may vary with time). This is a considerable simplification because it eliminates the dependence of ψ on $\underset{\sim}{x}$. While homogeneity may seem a restrictive condition, many flows of rheological interest, such as shear and extensional flows, satisfy this condition. Nevertheless, in this work we focus on the case of "weakly non-homogeneous" velocity fields, which are non-homogeneous flows in which the local homogeneity assumption applies (as opposed to "strongly non-homogeneous" flows).

Returning to Eq.(1.16), the "diffusion in physical space" term, $\frac{l_0^2}{8\lambda}\Delta_x\psi$ deserves some attention. The standard approach in the literature has been to discard this term outright because the coefficient is typically on the order of 10^{-7} to 10^{-9} (assuming our macroscopic length scale is on the order of 1 cm) [4]. However, it has been recognised by Barrett and Süli [2] that, with an eye toward proving existence and uniqueness of weak solutions, this simplification is counterproductive as when the term $\frac{l_0^2}{8\lambda}\Delta_x\psi$ is removed Eq.(1.16) becomes a degenerate parabolic equation that exhibits hyperbolic behaviour in physical space. Nevertheless, in this work we perform the standard model reduction as our main focus is on proposing a computational framework for the coupled NS–FP system, and retaining the physical space diffusion term would have negligible effect on computed solutions. As a result, the final form of the Fokker–Planck equation for the distribution of dumbbell configurations in a dilute polymeric solution is:

$$\frac{\partial \psi}{\partial t} + (\underset{\sim}{u} \cdot \underset{\sim}{\nabla}_x)\psi + \underset{\sim}{\nabla}_q \cdot \left(\left(\underset{\approx}{\kappa}\underset{\sim}{q} - \frac{1}{2\lambda}\underset{\sim}{F}(\underset{\sim}{q}) \right) \psi \right) = \frac{1}{2\lambda}\Delta_q\psi, \tag{1.17}$$

for $\psi : (\underset{\sim}{x}, \underset{\sim}{q}, t) \in \Omega \times D \times (0, T] \to \psi(\underset{\sim}{x}, \underset{\sim}{q}, t) \in \mathbb{R}$. We supplement (1.17) with an initial condition $\psi(\underset{\sim}{x}, \underset{\sim}{q}, 0) = \psi_0(\underset{\sim}{x}, \underset{\sim}{q})$ and appropriate boundary conditions.

The behaviour of Eq.(1.17) is very different in physical space compared to configuration space and the boundary conditions must reflect this. In configuration space Eq.(1.17) is a parabolic equation and we typically impose a zero-Dirichlet boundary condition on $\Omega \times \partial D$ as a dumbbell cannot realise the upper bound on its length. On the other hand, in physical space the equation is hyperbolic so letting $\partial\Omega^-$ denote the inflow part of the boundary, we only impose a boundary condition on $\partial\Omega^- \times D$. However, in order to impose a boundary condition at inflow one must know ψ upstream from the boundary. One solution is to enforce a periodic boundary condition so that the "upstream" flow is effectively contained in Ω. Alternatively, one could assume a

fully developed flow upstream so that the configuration distribution for this flow can be determined and convected into Ω.

To take into account the fact that the mass in the dumbbell model is in the beads rather than at the centre of mass, Biller and Petruccione [5] defined the *polymer number density*, $n_p(\underset{\sim}{x},t)$, (which denotes the dumbbell concentration at $(\underset{\sim}{x},t)\in\Omega\times(0,T]$), as:

$$n_p(\underset{\sim}{x},t)=\int_D \psi(\underset{\sim}{x}+l_0\underset{\sim}{q}/2,\underset{\sim}{x},t)\mathrm{d}\underset{\sim}{q}.$$

By the local homogeneity assumption we can write the Taylor series for ψ up to the linear term, and obtain:

$$n_p(\underset{\sim}{x},t)=\int_D \psi(\underset{\sim}{x},\underset{\sim}{q},t)\mathrm{d}\underset{\sim}{q}+\int_{\mathrm{D}}\frac{\mathrm{l}_0}{2}\underset{\sim}{q}\cdot\underset{\sim}{\nabla}_{\mathrm{q}}\psi(\underset{\sim}{x},\underset{\sim}{q},\mathrm{t})\mathrm{d}\underset{\sim}{q}. \tag{1.18}$$

The second term on the right-hand-side of Eq.(1.18) is zero since ψ is symmetric about the origin. Hence, under the local homogeneity assumption for ψ, n_p reduces to:

$$n_p(\underset{\sim}{x},t)=\int_D \psi(\underset{\sim}{x},\underset{\sim}{q},t)\mathrm{d}\underset{\sim}{q}. \tag{1.19}$$

We now proceed to show that n_p is conserved. Integrating Eq.(1.17) in configuration space we obtain:

$$\frac{\partial}{\partial t}\int_D \psi\mathrm{d}\underset{\sim}{q}=-\int_{\mathrm{D}}\underset{\sim}{u}\cdot\underset{\sim}{\nabla}_{\mathrm{x}}\psi\mathrm{d}\underset{\sim}{q}-\int_{\mathrm{D}}\underset{\sim}{\nabla}_{\mathrm{q}}\cdot\left(\left(\underset{\approx}{\kappa}\underset{\sim}{q}-\frac{1}{2\lambda}\underset{\sim}{F}(\underset{\sim}{q})\right)\psi\right)\mathrm{d}\underset{\sim}{q}+\frac{1}{2\lambda}\int_{\mathrm{D}}\Delta_{\mathrm{q}}\psi\mathrm{d}\underset{\sim}{q}.$$

Integrating the first term on the right by parts, and applying the divergence theorem to the second and third terms gives,

$$\begin{aligned}\frac{\partial}{\partial t}\int_D \psi\mathrm{d}\underset{\sim}{q} &= \int_D \psi(\underset{\sim}{\nabla}_x\cdot\underset{\sim}{u})\mathrm{d}\underset{\sim}{q}-\int_{\partial D}\psi\,(\underset{\sim}{u}\cdot\underset{\sim}{n})\,\mathrm{d}s\\ &\quad-\int_{\partial D}\psi\left(\left(\underset{\approx}{\kappa}\underset{\sim}{q}-\frac{1}{2\lambda}\underset{\sim}{F}(\underset{\sim}{q})\right)\cdot\underset{\sim}{n}\right)\mathrm{d}s+\frac{1}{2\lambda}\int_{\partial D}(\underset{\sim}{\nabla}_q\psi)\cdot\underset{\sim}{n}\mathrm{d}s\end{aligned}$$

in which all the terms on the right-hand side vanish; the first term because the solvent is incompressible, and the other three because both ψ and $\underset{\sim}{\nabla}_q\psi$ decay to zero as $|\underset{\sim}{q}|\to\sqrt{b}$ for FENE dumbbells or as $|\underset{\sim}{q}|\to\infty$ for Hookean dumbbells. So we can see that $n_p(\underset{\sim}{x},t)$ is constant in time at any point $\underset{\sim}{x}$ in physical space. We assume that n_p is constant throughout physical space and scale ψ by this constant so that it satisfies the normalisation condition for a pdf:

$$\int_D \psi(\underset{\sim}{x},\underset{\sim}{q},t)\mathrm{d}\underset{\sim}{q}=1. \tag{1.20}$$

Finally, we consider how ψ should behave at solid walls. Strictly speaking proximity to a solid wall will reduce the space of possible configurations a dumbbell can realise, i.e. configuration space depends on the position in physical space:

$$D(\underset{\sim}{x})=\{\underset{\sim}{q}:|\underset{\sim}{q}|<Q_{max}\}\cap\{\underset{\sim}{q}:\underset{\sim}{x}\pm l_0\underset{\sim}{q}/2\in\Omega\}.$$

Another complication analysed by Biller and Petruccione [5] is that solid walls may affect the concentration of polymers in the fluid so that the polymer number density n_p need not be constant throughout Ω. In particular, Biller and Petruccione considered the shear flow of a dilute polymer solution in a channel of width comparable to l_0. In this situation the polymer number density varies depending on proximity to the channel walls and one must introduce an "impenetrable wall" boundary condition to ensure $n_p(\underset{\sim}{x}, t)$ is modelled accurately. Supposing we have an impenetrable wall with unit normal $\underset{\sim}{n}$, then it is characterised by the following boundary condition (expressed in terms of bead positions $\underset{\sim}{r}_i = (x_i, y_i, z_i)$):

$$kT(\underset{\sim}{\nabla}_{r_i}\psi^{12} \cdot \underset{\sim}{n}) + (\underset{\sim}{F}(\underset{\sim}{r}_i + \underset{\sim}{r}_j) \cdot \underset{\sim}{n})\psi^{12} = 0 \text{ for } i, j = 1, 2; i \neq j. \tag{1.21}$$

As indicated in Section 4.5 of [25], these more subtle considerations are only relevant in strongly non-homogeneous flows in which the local homogeneity assumption is not applicable (such as the narrow channel shear flow in [5]). In our work, however, we only consider "weakly non-homogeneous" flows and hence we can ignore the two complications mentioned above. We treat D as be independent of $\underset{\sim}{x} \in \Omega$, and we do not impose the more complex boundary condition of Eq.(1.21). Instead, if $x \in \partial\Omega$ is on a solid wall then we impose a no-slip condition on the velocity $\underset{\sim}{u}$ and allow this no-slip velocity to convect ψ in physical space as in Eq.(1.17).

1.5.2 The polymeric extra stress

The purpose of deriving Eq.(1.17) was so that we could use it to compute the extra-stress tensor $\underset{\approx}{\tau}(\underset{\sim}{x}, t)$, a macroscopic quantity that feeds into the Navier–Stokes equations as a source term. There are two components that contribute to this tensor, $\underset{\approx}{\tau}^C$, which is due to spring tension, and $\underset{\approx}{\tau}^K$ which arises from bead motion. Due to the equilibrium in momentum space assumption, $\underset{\approx}{\tau}^K$ is isotropic and takes the form [7]:

$$\underset{\approx}{\tau}^K = -2n_p kT \underset{\approx}{I}. \tag{1.22}$$

Biller and Petruccione [5] derived $\underset{\approx}{\tau}^C$ in the case of a non-homogeneous velocity field which, if we utilise the local homogeneity assumption on ψ, is given by:

$$\underset{\approx}{\tau}^C(\underset{\sim}{x}, t) = n_p kT \int_D \underset{\sim}{q} \otimes \underset{\sim}{F}(\underset{\sim}{q})\psi(\underset{\sim}{x}, \underset{\sim}{q}, t)\mathrm{d}\underset{\sim}{q} \tag{1.23}$$

Before combining Eqs. (1.22) and (1.23) we note that in equilibrium (i.e. when $\underset{\approx}{\kappa} = 0$), we have $\underset{\approx}{\tau} = -n_p kT \underset{\approx}{I}$ [7]. By convention, in non-equilibrium flows we separate this isotropic equilibrium stress from $\underset{\approx}{\tau}$ and absorb it into the pressure term [25]. This has no effect on the dynamics of the incompressible fluid, for which only $\underset{\sim}{\nabla}_x p$ is relevant. As a result, our expression for the stress tensor is:

$$\underset{\approx}{\tau}(\underset{\sim}{x}, t) = n_p kT \left(-\underset{\approx}{I} + \int_D \underset{\sim}{q} \otimes \underset{\sim}{F}(\underset{\sim}{q})\psi(\underset{\sim}{x}, \underset{\sim}{q}, t)\mathrm{d}\underset{\sim}{q} \right). \tag{1.24}$$

This equation is known as the *Kramers expression* for the polymeric extra-stress. From Eq.(1.24), we can see that $\underset{\approx}{\tau}$ is symmetric.

For our purposes it will be useful to express Eq.(1.24) in terms of the *polymeric viscosity*, η_p, which is defined analogously to the viscosity of a Newtonian liquid. For the Hookean dumbbell model in shear flow with shear rate $\dot{\gamma}$ it can be shown [7] that,

$$\tau_{xy} = \dot{\gamma}\lambda n_p kT,$$

and for the FENE dumbbell model, the shear stress is approximated by:

$$\tau_{xy} \approx \dot{\gamma}\lambda n_p kT \left(\frac{b+d+2}{b}\right).$$

Hence the polymeric viscosity is defined as:

$$\eta_p = \begin{cases} \lambda n_p kT & \text{for Hookean dumbbells} \\ \lambda n_p kT \left(\frac{b+d+2}{b}\right) & \text{for } d\text{-dimensional FENE dumbbells} \end{cases}$$

Rewriting Eq.(1.24) using these definitions, we get:

$$\underset{\approx}{\tau}(\underset{\sim}{x},t) = \frac{\eta_p}{\lambda}\left(-\underset{\approx}{I} + \int_D \underset{\sim}{q}\otimes\underset{\sim}{F}(\underset{\sim}{q})\psi(\underset{\sim}{x},\underset{\sim}{q},t)\mathrm{d}\underset{\sim}{q}\right), \tag{1.25}$$

for Hookean dumbbells and

$$\underset{\approx}{\tau}(\underset{\sim}{x},t) = \frac{\eta_p}{\lambda}\left(\frac{b+d+2}{b}\right)\left(-\underset{\approx}{I} + \int_D \underset{\sim}{q}\otimes\underset{\sim}{F}(\underset{\sim}{q})\psi(\underset{\sim}{x},\underset{\sim}{q},t)\mathrm{d}\underset{\sim}{q}\right), \tag{1.26}$$

for FENE dumbbells.

Now that we have derived the coupled NS–FP system and can compute $\underset{\approx}{\tau}$ we are ready to move on to computational approaches to solving this micro-macro system.

2 Computational approaches to polymer fluid dynamics

In Section 2.1 we give a summary of historical developments in computational modelling of polymeric fluids, which draws on the survey article by Keunings [21]. A number of different approaches have been popular in the literature; fully macroscopic approaches, various methods using stochastics in dealing with the micro-macro equations, and more recently some work has been done with fully deterministic approaches to multiscale models. In Section 2.2 we present our approach, which is to employ a deterministic finite element technique to solve the coupled Navier–Stokes and Fokker–Planck system of PDEs.

2.1 Literature review

Pioneering work in computational rheology began around 1970. By necessity, this early work relied on the fully macroscopic approach discussed in Section 1 as it is far less computationally expensive than a micro-macro method. A macroscopic computation typically employs standard tools of computational fluid dynamics, such as finite elements, finite volumes and spectral methods. This is a vast area of research still actively being developed. See the review article by Keunings [20] for an informative summary.

The alternative approach that has gained popularity since the early 1990s is to treat the multiscale equations (i.e. coupled NS and FP equations from Section 1) directly. A seminal idea in this direction was proposed by Öttinger and Laso in 1992 [24], who implemented a stochastic solver to model the dynamics of polymer molecules in a flow and coupled this to a finite element simulation of the macroscopic flow. This approach, known by the imposing acronym CONNFFESSIT (for "**C**alculation **o**f **N**on-**N**ewtonian **F**low: **F**inite **E**lements and **S**tochastic **Si**mulation **T**echnique"), was thoroughly developed and improved upon throughout the 1990s and has been successfully applied to a range of flows and polymer models. Subsequent research in this area has led to a family of techniques we refer to as "stochastic approaches". Along with the CONNFFESSIT idea, this includes the method of Brownian configuration fields [18] and the Lagrangian particle method [17].

The central idea of a stochastic approach, as detailed in [30], is to exploit the equivalence between the Fokker–Planck equation, Eq.(1.17), and the following Itô stochastic differential equation:

$$\mathrm{d}\underset{\sim}{q}(\underset{\sim}{x},t) + \underset{\sim}{u}(\underset{\sim}{x},t)\cdot\underset{\sim}{\nabla}_x\underset{\sim}{q}(\underset{\sim}{x},t)\mathrm{d}t = \left(\underset{\approx}{\kappa}(\underset{\sim}{x},t)\underset{\sim}{q}(\underset{\sim}{x},t) - \frac{1}{2\lambda}\underset{\sim}{F}(\underset{\sim}{q}(\underset{\sim}{x},t))\right)\mathrm{d}t + \sqrt{\frac{1}{\lambda}}\mathrm{d}\underset{\sim}{W}(\underset{\sim}{x},t).$$

This stochastic differential equation is solved using a Monte-Carlo approach in which initially a large number of model polymer molecules are distributed throughout the computational domain and their motion is subsequently tracked as they are convected along streamlines and stretched and oriented by the flow. The Navier–Stokes equations must be solved to determine the macroscopic velocity field, typically using finite-elements or some other standard CFD tool. The stress field is updated at each time step by computing an ensemble average for the molecules located in each finite element. The stochastic approach is a computationally intensive procedure – it is little wonder there was no work done in this direction prior to the 1990s. Moreover, a drawback of the stochastic approach is that it introduces a slowly decaying stochastic error (typically $O(N^{-1/2})$ as $N \to \infty$). Variance reduction techniques were developed to ameliorate this error term and reduce the number of polymer molecules one must track in order to compute an ensemble average to within a given error tolerance (see [21] for an overview of variance reduction in this context). However, even with variance reduction techniques, the presence of stochastic error is a significant limitation of the stochastic approach and circumventing this is an important motivation for moving to deterministic methods. On the other hand, an important advantage of the stochastic approach is that it scales well with the number of degrees of freedom in the polymer model; indeed computations have

been carried out with models with $O(10^2)$ degrees of freedom [21].

The multiscale approach that we advocate in this work is to solve for both the velocity field, $\underset{\sim}{u}(\underset{\sim}{x},t)$, and the polymer configuration pdf, $\psi(\underset{\sim}{x},\underset{\sim}{q},t)$, deterministically. The major challenge of this approach is to deal with the high-dimensionality of the Fokker–Planck equation which, for a non-homogeneous 3D flow of a dumbbell suspension, is 6-dimensional. Of course the dimensionality increases if we seek to use mechanical models with more degrees of freedom. Comparatively little work has been done using this approach and it is most likely the high-dimensionality that has discouraged attempts to solve the FP equation directly. Stewart and Sørensen in 1972 [32] used spherical harmonics to solve the Fokker–Planck equation for a steady shear flow of a dilute suspension of rigid dumbbells. Warner [34] applied a similar approach to the study of shear flows of FENE dumbbells and this work was improved upon 13 years later by Fan [14]. These early studies considered the simplified case of homogeneous flows so that ψ is a function of $\underset{\sim}{q}$ and t only. The first work utilising a deterministic approach to solve a non-homogeneous velocity field was by Fan in 1989 [15] who simulated a planar channel flow using a bead-rod polymer model. Use of the bead-rod model in Fan's computation meant that configuration space was 2-dimensional. Also, although ψ was dependent on $\underset{\sim}{x}$, Fan made the simplifying assumption that the physical space convection term, $\underset{\sim}{u}\cdot\underset{\sim}{\nabla}_x\psi$, vanished. Fan's work was subsequently extended by eliminating the assumption that the convection term vanishes; Nayak [28] treated convection in physical space using a discontinuous Galerkin method, whereas Grosso *et. al.* [16] used a streamline-diffusion method.

In a series of papers published since 2003 by Lozinski, Chauvière and other collaborators [10, 11, 25–27], the state-of-the-art of the deterministic approach has been considerably advanced. An important technique used by these authors is to split each time step of the Fokker–Planck equation into two sub-steps:

$$\frac{\tilde{\psi}-\psi^n}{\Delta t}+\underset{\sim}{\nabla}_q\cdot\left(\left(\underset{\approx}{\kappa}^n\underset{\sim}{q}-\frac{1}{2\lambda}\underset{\sim}{F}(\underset{\sim}{q})\right)\tilde{\psi}\right) = \frac{1}{2\lambda}\Delta_q\tilde{\psi}, \tag{2.1a}$$

$$\frac{\psi^{n+1}-\tilde{\psi}}{\Delta t}+\underset{\sim}{u}^n\cdot\underset{\sim}{\nabla}_x\psi^{n+1} = 0, \tag{2.1b}$$

where $\tilde{\psi}$ is the intermediate value, and $\underset{\sim}{u}^n$ and $\underset{\approx}{\kappa}^n=(\underset{\sim}{\nabla}_x\underset{\sim}{u}^n)$ are evaluated at time-level n. We utilise this operator splitting technique in our finite element based approach to solving the Fokker–Planck equation (see Section 2.2.2). Using this technique for, say, a non-homogeneous 3D flow, means that we solve a series of 3-dimensional problems rather than the full 6-dimensional Fokker–Planck equation. By reducing the dimension in this fashion we mitigate the impact of the so-called "curse of dimensionality", which refers to the exponential growth of the number of grid points in a mesh (and hence computational complexity of the problem) as the dimension is increased.

Lozinski and Chauvière [10,11,26] demonstrated that for the FENE dumbbell model their deterministic method can outperform stochastic approaches on some benchmark flows. In particular, they considered a planar flow in a channel with a circular obstacle, such that physical space was 2-dimensional. For simplicity it was also assumed that

configuration space was 2-dimensional in [11, 26], even though there is no reason that polymer motion should also be confined to a plane. Thus in essence a 4-dimensional FP equation was solved. In [10], the same problem was considered but configuration space was taken to be 3-dimensional and interestingly the results showed good agreement with the case when D was taken to be 2-dimensional. They compared a stochastic approach to their deterministic method for this problem and demonstrated that the deterministic approach was significantly more efficient in terms of computational cost, and it was also more accurate due to the absence of stochastic error. The results of Lozinski *et. al.* demonstrate that a deterministic approach can outperform stochastic methods for models with low dimensional configuration space, but it is still an open questions whether the deterministic approach can be competitive for models with configuration space dimension greater than 3.

2.2 Deterministic algorithm for micro-macro model

In this section we discuss our numerical approach to solving the coupled Fokker–Planck and Navier–Stokes micro-macro system. We note that Barrett, Schwab and Süli [1] and Barrett and Süli [2] have proved results for the existence and uniqueness of weak solutions for this system.

2.2.1 Numerical approach for the Navier–Stokes system

First let us consider the Navier–Stokes equations. For simplicity we set $\rho = 1$ in Eq.(1.6a) and, following [8], the weak formulation of Eqs.(1.6a) and (1.6b) is to find $\underset{\sim}{u} \in \underset{\sim}{V} = H^1(\Omega)^d$ and $p \in \Pi = \{q \in L^2(\Omega) : \int_\Omega q \mathrm{d}\underset{\sim}{x} = 0\}$ such that:

$$\begin{aligned}\int_\Omega \frac{\partial \underset{\sim}{u}}{\partial t} \cdot \underset{\sim}{v} \mathrm{d}\underset{\sim}{x} \;&+\; \eta_s \int_\Omega \underset{\sim}{\nabla}_x \underset{\sim}{u} : \underset{\sim}{\nabla}_x \underset{\sim}{v} \mathrm{d}\underset{\sim}{x} - \int_\Omega (\underset{\sim}{\nabla}_x \cdot \underset{\sim}{v}) p \mathrm{d}\underset{\sim}{x} \\ &+\; \int_\Omega (\underset{\sim}{u} \cdot \underset{\sim}{\nabla}_x \underset{\sim}{u}) \cdot \underset{\sim}{v} \mathrm{d}\underset{\sim}{x} + \int_\Omega \underset{\approx}{\tau} : \underset{\sim}{\nabla}_x \underset{\sim}{v} \mathrm{d}\underset{\sim}{x} = 0, \end{aligned} \tag{2.2}$$

and

$$\int_\Omega (\underset{\sim}{\nabla}_x \cdot \underset{\sim}{u}) q \mathrm{d}\underset{\sim}{x} = 0, \tag{2.3}$$

for all $\underset{\sim}{v} \in \underset{\sim}{V}$ and $q \in \Pi$, and where $\underset{\approx}{A} : \underset{\approx}{B} = \sum A_{ij} B_{ij}$. As discussed in Section 1, the polymeric extra stress tensor $\underset{\approx}{\tau}$ is computed from the solution of the Fokker–Planck equation. It is through this term that the microscopic and macroscopic equations are coupled together. In this section we take $\underset{\approx}{\tau}$ as a given source term. Details on numerically solving the FP equation and computing $\underset{\approx}{\tau}$ are presented in Section 2.2.2.

In order to implement the weak form of the NS equations using the finite-element method, we break each of Eqs. (2.2) and (2.3) into three equations, one for each component of $\underset{\sim}{u} = (u_x, u_y, u_z)$ where u_x is the x-component of the velocity field. Then for u_x

we have; find $u_x \in V = H^1(\Omega)$ and $p \in \Pi$ such that:

$$\begin{aligned}\int_\Omega \frac{\partial u_x}{\partial t} v_x \mathrm{d}\underset{\sim}{x} &+ \eta_s \int_\Omega \underset{\sim}{\nabla}_x u_x \cdot \underset{\sim}{\nabla}_x v_x \mathrm{d}\underset{\sim}{x} - \int_\Omega p \frac{\partial v_x}{\partial x} \mathrm{d}\underset{\sim}{x} \\ &+ \int_\Omega \left(\underset{\sim}{u} \cdot \underset{\sim}{\nabla}_x u_x\right) v_x \mathrm{d}\underset{\sim}{x} + \int_\Omega \left(\tau_{xx}\frac{\partial v_x}{\partial x} + \tau_{xy}\frac{\partial v_x}{\partial y} + \tau_{xz}\frac{\partial v_x}{\partial z}\right) \mathrm{d}\underset{\sim}{x} \\ &= 0, \end{aligned} \tag{2.4}$$

and

$$\int_\Omega q \frac{\partial u_x}{\partial x} \mathrm{d}\underset{\sim}{x} = 0, \tag{2.5}$$

for all $v_x \in V$ and $q \in \Pi$. Of course, Eqs. (2.4) and (2.5) are coupled to analogous equations for u_y and u_z.

Let $\{\phi_1, \phi_2, \ldots, \phi_N\}$ be a basis of the finite-dimensional subspace V^h of V, and similarly $\mathrm{span}\{\psi_1, \psi_2, \ldots, \psi_{N'}\} = \Pi^h$. For stability of the mixed method (i.e. in order to satisfy the "inf-sup" condition [8]), we choose V^h to be a space of continuous piece-wise quadratic functions, and Π^h a space of piece-wise linear functions. Discretising in space and in time so that a superscript n indicates a value at $t = t^n = n\Delta t$, we obtain $U_x^n(\underset{\sim}{x}) = \sum_j u_x^{n,j}\phi_j(\underset{\sim}{x})$ and $P^n(\underset{\sim}{x}) = \sum_j p^{n,j}\psi_j(\underset{\sim}{x})$, where the variables have been capitalised to indicate discretisation. Substituting U_x^n and P^n into Eqs.(2.4) and (2.5) and using the backward-Euler method in time to ensure that we have no constraint on time step size for stability, the discretised variational problem takes the form; for each $n = 0, \ldots, M$, where $M = T/\Delta t$, find $\underset{\sim}{X}^n = (\underset{\sim}{u}_x^n, \underset{\sim}{u}_y^n, \underset{\sim}{u}_z^n, \underset{\sim}{p}^n)^T \in \mathbb{R}^{3N+N'}$ such that:

$$\begin{aligned} F_x^i(\underset{\sim}{X}^{n+1}) &= \sum_{j=1}^N u_x^{n+1,j} \int_\Omega \left(\phi_j\phi_i + \Delta t \eta_s \left(\underset{\sim}{\nabla}_x\phi_j \cdot \underset{\sim}{\nabla}_x\phi_i\right)\right) \mathrm{d}\underset{\sim}{x} \\ &\quad + \Delta t \int_\Omega \left[\left(\sum_{j=1}^N u_x^{n+1,j}\phi_j\right)\left(\sum_{j=1}^N u_x^{n+1,j}\frac{\partial\phi_j}{\partial x}\right)\right. \\ &\qquad + \left(\sum_{j=1}^N u_y^{n+1,j}\phi_j\right)\left(\sum_{j=1}^N u_x^{n+1,j}\frac{\partial\phi_j}{\partial y}\right) \\ &\qquad \left. + \left(\sum_{j=1}^N u_z^{n+1,j}\phi_j\right)\left(\sum_{j=1}^N u_x^{n+1,j}\frac{\partial\phi_j}{\partial z}\right)\right] \phi_i \mathrm{d}\underset{\sim}{x} \\ &\quad + \Delta t \int_\Omega \tau_{xx}\frac{\partial\phi_i}{\partial x} + \tau_{xy}\frac{\partial\phi_i}{\partial y} + \tau_{xz}\frac{\partial\phi_i}{\partial z} \mathrm{d}\underset{\sim}{x} \\ &\quad - \Delta t \sum_{j=1}^{N'} p_j^{n+1} \int_\Omega \psi_j \frac{\partial\phi_i}{\partial x} \mathrm{d}\underset{\sim}{x} - \sum_{j=1}^N \int_\Omega u_x^{n,j}\phi_j\phi_i \mathrm{d}\underset{\sim}{x} = 0, \end{aligned} \tag{2.6}$$

and

$$G_x^{i'}(\underset{\sim}{X}^{n+1}) = \sum_{j=1}^N u_x^{n+1,j} \int_\Omega \psi_{i'} \frac{\partial\phi_j}{\partial x} \mathrm{d}\underset{\sim}{x} = 0, \tag{2.7}$$

for all $\phi_i, i = 1, \ldots, N$ and $\psi_{i'}, i' = 1, \ldots, N'$. For convenience we have labelled the left-hand-sides of Eqs.(2.6) and (2.7) as $F_x^i(\underset{\sim}{X}^{n+1})$ and $G_x^{i'}(\underset{\sim}{X}^{n+1})$ respectively, and we define $F_y^i(\underset{\sim}{X}^{n+1})$, $F_z^i(\underset{\sim}{X}^{n+1})$ and $G_y^{i'}(\underset{\sim}{X}^{n+1})$, $G_z^{i'}(\underset{\sim}{X}^{n+1})$ as the analogous equations for u_y and u_z. Eqs.(2.6) and (2.7) and their analogues each define a vector, e.g. $\underset{\sim}{F}_x(\underset{\sim}{X}) = (F_x^1(\underset{\sim}{X}), \ldots, F_x^N(\underset{\sim}{X}))^T \in \mathbb{R}^N$. We conflate $\underset{\sim}{G}_x, \underset{\sim}{G}_y, \underset{\sim}{G}_z \in \mathbb{R}^{N'}$ into a single vector, $\underset{\sim}{G} \in \mathbb{R}^{N'}$, given by:

$$G^{i'}(\underset{\sim}{X}^{n+1}) = \sum_{j=1}^{N} \left(u_x^{n+1,j} \int_\Omega \psi_{i'} \frac{\partial \phi_j}{\partial x} \mathrm{d}\underset{\sim}{x} + u_y^{n+1,j} \int_\Omega \psi_{i'} \frac{\partial \phi_j}{\partial y} \mathrm{d}\underset{\sim}{x} + u_z^{n+1,j} \int_\Omega \psi_{i'} \frac{\partial \phi_j}{\partial z} \mathrm{d}\underset{\sim}{x} \right) = 0.$$

Let $\underset{\sim}{H} = (\underset{\sim}{F}_x, \underset{\sim}{F}_y, \underset{\sim}{F}_z, \underset{\sim}{G})^T \in \mathbb{R}^{3N+N'}$. In order to compute the solution of the discrete NS system at time level $n+1$, we seek a solution of the non-linear system of equations $\underset{\sim}{H}(\underset{\sim}{X}^{n+1}) = \underset{\sim}{0}$. We use Newton's method to solve this system. Let J denote the Jacobian of the system. We calculate the entries of the matrix J by differentiating $\underset{\sim}{H}(\underset{\sim}{X}^{n+1})$ with respect to the components of $\underset{\sim}{X}^{n+1}$. Suppose we arrange our solution vector $\underset{\sim}{X}^{n+1}$ so that its first N entries are those of the vector $\underset{\sim}{u}_x^{n+1}$ then for $1 \leq i, j \leq N$, we have:

$$J_{ij} = \frac{\partial F_x^i(\underset{\sim}{X}^{n+1})}{\partial u_x^{n+1,j}} = \int_\Omega \phi_j \phi_i + \Delta t \left(\eta_s \left(\underset{\sim}{\nabla}_x \phi_j \cdot \underset{\sim}{\nabla}_x \phi_i \right) + \left(\phi_j \frac{\partial u_x^{n+1}}{\partial x} + \underset{\sim}{u}_x^{n+1} \cdot \underset{\sim}{\nabla}_x \phi_j \right) \phi_i \right) \mathrm{d}\underset{\sim}{x}.$$

The other entries of J are computed in a similar fashion. Now, supposing our previous (i.e. k^{th}) iterate for the solution at time t^n is $\underset{\sim}{X}_k^n$, then using Newton's method we have:

$$J\underset{\sim}{X}_{k+1}^{n+1} = J\underset{\sim}{X}_k^{n+1} - \underset{\sim}{H}(\underset{\sim}{X}_k^{n+1}). \tag{2.8}$$

We take the solution from the previous time step as our initial guess, $\underset{\sim}{X}_0^{n+1}$, and iteratively update $\underset{\sim}{X}_k^{n+1}$ until $||\underset{\sim}{X}_{k+1}^{n+1} - \underset{\sim}{X}_k^{n+1}|| < \mathrm{TOL}$ is satisfied for some pre-defined tolerance TOL.

2.2.2 Numerical approach for the Fokker–Planck equation

In this section we present a finite element based method for solving Eq.(1.17). First we perform the operator splitting step described in Section 2.1 to obtain two equations: the configuration space equation, Eq.(2.1a), and the physical space equation, Eq.(2.1b). Notice that these equations have been discretised in time using the backward Euler scheme. As in the Navier–Stokes case this is to ensure that we have no constraint on time step size. There is no advantage in using the Crank-Nicolson method for the Fokker–Planck equation because the velocity field is computed at $t = t^n$, not $t = t^{n+1/2}$, so we would not obtain second-order convergence in time anyway. We henceforth focus our attention on the 3D FENE dumbbell model, although analogous results hold for the 2D FENE case, and for the Hookean dumbbell model. For 3D FENE dumbbells, $\underset{\sim}{F}(\underset{\sim}{q})$ is given by Eq.(1.14), and $D = B(0, \sqrt{b}) \subset \mathbb{R}^3$.

On putting Eq.(2.1a) into weak form the problem in configuration space becomes:

find $\tilde{\psi} \in K$ such that:

$$\int_D \tilde{\psi} v \mathrm{d}\underset{\sim}{q} + \frac{\Delta t}{2\lambda} \int_D \underset{\sim}{\nabla}_q \tilde{\psi} \cdot \underset{\sim}{\nabla}_q v \mathrm{d}\underset{\sim}{q} + \Delta t \int_D \underset{\sim}{\nabla}_q \cdot \left(\left(\underset{\approx}{\kappa}^n \underset{\sim}{q} - \frac{1}{2\lambda} \underset{\sim}{F}(\underset{\sim}{q}) \right) \tilde{\psi} \right) v \mathrm{d}\underset{\sim}{q} = \int_D \psi^n v \mathrm{d}\underset{\sim}{q},$$

for all $v \in K$. The boundary term arising from integrating the diffusion term by parts vanishes in Eq.(2.9) because of the Dirichlet condition $\psi|_{\partial D} = 0$. Also, due to the modelling assumption that the two beads of a dumbbell are indistinguishable, the solution of this PDE will be symmetric with respect to the origin. See [1, 2] for details on the correct choice of function space K for this variational problem.

In order to solve Eq.(2.9) numerically, it is natural to transform to spherical coordinates to represent the domain D, i.e. $\underset{\sim}{q} = (\rho \cos\theta \sin\varphi, \rho \sin\theta \sin\varphi, \rho \cos\varphi)$ for $(\rho, \theta, \varphi) \in [0, \sqrt{b}] \times [0, 2\pi] \times [0, \pi]$. On changing to spherical coordinates it is necessary to impose a periodic boundary condition on θ since a 2π rotation in θ is the identity operator. We follow Chauvière and Lozinski [11] in introducing the following ansatz for ψ:

$$\psi(\underset{\sim}{x}, \rho, \theta, \varphi, t) = \Psi_0 \alpha(\underset{\sim}{x}, \rho, \theta, \varphi, t), \tag{2.9}$$

where $\Psi_0 = (1 - \rho^2/b)^s$ and s is a positive constant. If s is set appropriately this substitution imposes the zero-Dirichlet condition, $\psi = 0$ at ∂D, in a numerically stable way despite the singularity introduced by $\underset{\sim}{F}$ at $\rho = \sqrt{b}$. In agreement with [10], we have found empirically that $s = 2.5$ gives a stable numerical scheme and this value was used to obtain the results in Section 3.

Moreover, as a consequence of the modelling assumption that the two beads of a dumbbell are indistinguishable, we require ψ to be symmetric with respect to the origin, i.e. $\psi(\rho, \theta, \varphi) = \psi(\rho, \theta + \pi, \pi - \varphi)$, but this symmetry is a natural consequence of the PDE

We are now ready to discuss the implementation of the finite element method for our system. Let K_α be the function space $K_\alpha = \{\alpha : \Psi_0 \alpha \in K\}$ and suppose $K_{\alpha,h}$ is a finite-dimensional subspace of K_α with basis $\{\phi_1, \ldots, \phi_N\}$. We obtain the spatially discretised version of Eq.(2.9) in terms of α by carrying out the following steps; (i) make the substitution Eq.(2.9), (ii) set $\tilde{\alpha}_h = \sum_j \tilde{\alpha}_j \phi_j$, (iii) set $v = \phi_i$, and (iv) evaluate the integrals over the domain $(\eta, \theta, \varphi) \in [-1, 1] \times [0, 2\pi] \times [0, \pi]$. With these operations we obtain the following system of equations:

$$\sum_{j=1}^{N} \tilde{\alpha}_j \int_{-1}^{1} \int_0^{2\pi} \int_0^{\pi} \left[\Psi_0 \phi_j \phi_i + \Delta t \left(\underset{\sim}{\nabla}_q \cdot \left(\left(\underset{\approx}{\kappa}^n \underset{\sim}{q} - \frac{1}{2\lambda} \underset{\sim}{F}(\underset{\sim}{q}) \right) \Psi_0 \phi_j \right) \phi_i + \frac{1}{2\lambda} \underset{\sim}{\nabla}_q (\Psi_0 \phi_j) \cdot \underset{\sim}{\nabla}_q \phi_i \right) \right] \rho^2 \sin\varphi \mathrm{d}\varphi \mathrm{d}\theta \mathrm{d}\eta = \int_{-1}^{1} \int_0^{2\pi} \int_0^{\pi} \Psi_0 \alpha^n \phi_i \rho^2 \sin\varphi \mathrm{d}\varphi \mathrm{d}\theta \mathrm{d}\eta \tag{2.10}$$

for $i = 1, 2, \ldots, N$.

Next we need to consider the physical space part of the Fokker–Planck equation, Eq.(2.1b). Making the substitution in Eq.(2.9), Ψ_0 can be factored from each term of this equation so the variational formulation becomes: find $\alpha^{n+1} \in W$ such that,

$$\int_\Omega \alpha^{n+1} v \mathrm{d}\underset{\sim}{x} + \Delta t \int_\Omega \left(\underset{\sim}{u}^n \cdot \underset{\sim}{\nabla}_x \alpha^{n+1}\right) v \mathrm{d}\underset{\sim}{x} = \int_\Omega \tilde{\alpha} v \mathrm{d}\underset{\sim}{x}, \tag{2.11}$$

for all $v \in W$. Imposing the finite element discretisations, $\alpha^h = \sum_j \alpha_j \phi_j$ and $v = \phi_i$, where $\mathrm{span}\{\phi_1, \ldots, \phi_N\} = W_h$, we obtain:

$$\sum_{j=1}^{N} \alpha_j^{n+1} \int_\Omega \left(\phi_j + \Delta t \left(\underset{\sim}{u}^n \cdot \underset{\sim}{\nabla}_x \phi_j\right)\right) \phi_i \mathrm{d}\underset{\sim}{x} = \int_\Omega \tilde{\alpha} \phi_i \mathrm{d}\underset{\sim}{x} \tag{2.12}$$

for $i = 1, 2, \ldots, N$. This is a straightforward Galerkin formulation of the hyperbolic equation. Based on the computations carried out so far (see Section 3) it appears that this simple approach is acceptable. However, it could be advantageous to use a stabilised method to discretise Eq.(2.11). Indeed Lozinski and Chauvière [11] used a spectral element based SUPG method, detailed in [12], for this purpose.

Note that Eq.(2.12) is independent of the position in configuration space. This is an important detail as it means that when implementing Eq.(2.12) in software we only have to assemble the system matrix once per time step. Unfortunately this property is not shared by Eq.(2.10), as $\underset{\approx}{\kappa}$ is a function of $\underset{\sim}{x}$ for a non-homogeneous velocity field.

Once ψ has been computed we need to use the Kramers expression to determine the polymeric extra stress, $\underset{\approx}{\tau}(\underset{\sim}{x}, t)$ for $(\underset{\sim}{x}, t) \in \Omega \times (0, T]$. This amounts to evaluating an integral over D, for which we need Kramers expression in terms of α:

$$\underset{\approx}{\tau}(\underset{\sim}{x}, t^n) = n_p kT \left(-\underset{\approx}{I} + \int_0^{\sqrt{b}} \int_0^{2\pi} \int_0^{\pi} \underset{\sim}{w} \otimes \underset{\sim}{w} \frac{\rho^4}{1 - \rho^2/b} \Psi_0 \alpha^n(\underset{\sim}{x}, \eta, \theta, \varphi) \sin\varphi \mathrm{d}\varphi \mathrm{d}\theta \mathrm{d}\rho \right),$$

where $\underset{\sim}{w} = (\cos\theta \sin\varphi, \sin\theta \sin\varphi, \cos\varphi)$.

2.3 Implementation of the numerical method

Our overall NS–FP solver can be broken down into distinct components; the Navier–Stokes solver, the Fokker–Planck configuration space solver, the Fokker–Planck physical space solver and the Kramers expression for computing $\underset{\approx}{\tau}$. We implemented each component using the C++ finite element library libMesh [22], which is a parallel, open source code developed at the University of Texas at Austin. The results of our computations using the libMesh library are presented in Section 3.

One important aspect of the implementation is how one should handle storage of the 6-dimensional solution of the FP equation, α. Our approach is straightforward; store α in a matrix in which each row contains a 3D cross-section of the solution in physical space corresponding to a fixed point in configuration space and similarly each column contains a cross-section in configuration space. α is then updated in by updating each cross-section sequentially.

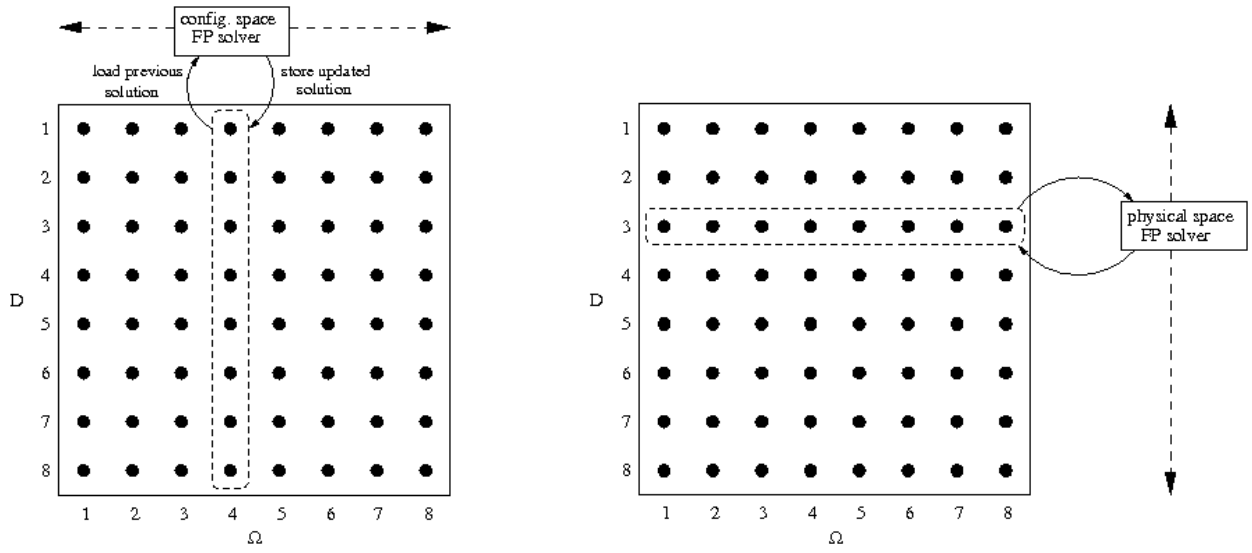

Figure 2: This schematic illustrates the operator splitting approach to solving the Fokker–Planck equation. In performing a single time step we first (a) update each configuration space cross section, and then (b) update each physical space cross section.

In the following listing we give a more precise description of the overall computational procedure:

1. Initialise the system to equilibrium by setting $\underset{\sim}{u}(\underset{\sim}{x},0) = \underset{\sim}{0}$ and $\psi(\underset{\sim}{x},\underset{\sim}{q},0) = \psi_{eq}(\underset{\sim}{q})$, where $\psi_{eq}(\underset{\sim}{q}) = C\left(1 - |\underset{\sim}{q}|^2/b\right)^{b/2}$ and C is a normalisation constant [7]. Also set $\underset{\approx}{\tau}(\underset{\sim}{x},0) = 0$ since the polymeric stress tensor vanishes in equilibrium.

2. Impose a non-zero flow condition through the boundary conditions on $\underset{\sim}{u}$ and update the velocity field using the Navier–Stokes solver outlined in Section (2.2.1).

3. Update α in D by iterating over the physical space mesh points and updating each configuration space cross-section using Eq.(2.10). The system matrix and right-hand-side vector must be reassembled for each point in physical space.

4. Update α in Ω for each mesh point in D using the Galerkin implementation given in Eq.(2.12). As mentioned previously, in this case it is only necessary to assemble the system matrix once per time step. This means that physical space updates take significantly less CPU time than configuration space updates, and the disparity grows with the problem size.

5. Compute $\underset{\approx}{\tau}$ based on the updated Fokker–Planck solution using Gaussian quadrature to evaluate the integral in Eq.(2.2.2).

6. Update $\underset{\sim}{u}$, which will be affected by the updated stress field. Return to Step 3 and repeat until a termination condition such as $\frac{||\underset{\sim}{u}^{n+1}-\underset{\sim}{u}^{n}||_\infty}{\Delta t} < \text{TOL}$ is met.

The majority of the time in this algorithm is spent updating α in configuration space. Optimising this step is a high priority. Lozinski and Chauvière introduced a "fast Fokker–Planck" solver in [26] which sped up the overall CPU time of their algorithm by a factor of more than 60. This was achieved by rearranging their spectral formulation of Eq.(2.9) to show that a number of matrices and matrix inverses could be pre-computed and reused in each solve, drastically reducing the work in each configuration space solve. However, this procedure is not well suited to a finite element approach as one of the primary advantages of the finite element method is that it allows us to deal exclusively with sparse linear algebra, but the inverse of a sparse matrix is generally dense so it is undesirable to compute explicit matrix inverses.

As a result we must look to other ways of speeding up the Fokker–Planck solver. One option is to utilise parallel computation. The libMesh library facilitates parallel computation and this approach has already yielded good results in making large-scale computations feasible (see Section 3). Another idea, discussed in Section 4, is to use sparse meshes to reduce the number of degrees of freedom in the configuration space mesh and hence reduce computation time.

3 Numerical results for homogeneous and non-homogeneous flows

In this section we present results of numerical simulations of polymeric flows computed using the finite element framework outlined in Section 2. We first consider some homogeneous flows in 2D and 3D before moving on to the much more challenging task of simulating non-homogeneous flows.

3.1 Homogeneous flows

A homogeneous flow is one in which the velocity gradient tensor, $\underset{\approx}{\kappa}$, is constant throughout Ω. Compared to non-homogeneous flows, this is a significant simplification. In a homogeneous flow the velocity field $\underset{\sim}{u}$ is assumed to be fixed so that we do not need to solve the NS equation, and also ψ does not depend on $\underset{\sim}{x}$. These simplifications mean that homogeneous flows are far more easily analysed both mathematically and numerically than non-homogeneous flows, and because of this there has been a great deal of work on homogeneous flows in the literature. For our purposes, it is useful to begin by considering homogeneous flows as that allows us to focus our attention on solving the isolated Fokker-Planck equation rather than the more complex FP–NS coupled system. In this section we present some numerical results for two canonical homogeneous flows; shear flows and extensional flows. Conveniently there are results available in the literature that we can compare our results to in order to verify the correctness of our FP solver.

3.2 Shear flows

A homogeneous shear flow has the velocity field $\underset{\sim}{u} = (\dot{\gamma}y, 0, 0)$, in which $\dot{\gamma}$ is the *shear rate*. The gradient of the shear velocity field is the constant tensor:

$$\underset{\approx}{\kappa} = \begin{pmatrix} 0 & \dot{\gamma} & 0 \\ 0 & 0 & 0 \\ 0 & 0 & 0 \end{pmatrix}. \tag{3.1}$$

First we present results for shear flows in which dumbbells are assumed to be confined to a plane. The exposition of the NS–FP system in Section 2 referred only to the 3-dimensional case. The 2D case that we consider here is analogous, except that we transform Eq.(2.9) using polar coordinates, $(q_1, q_2) = (\rho\cos\theta, \rho\sin\theta), \rho \in [0, \sqrt{b}], \theta \in [0, 2\pi]$, rather than spherical coordinates. Due to the symmetry of ψ about the origin, if we impose the periodic boundary condition $\psi(\rho, \theta, t) = \psi(\rho, \theta + \pi, t)$, then we need only consider the domain $(\rho, \theta) \in [0, \sqrt{b}] \times [0, \pi]$. This is the approach adopted in this section.

In Figure 3, we plot the steady state solution, $\alpha(\rho, \theta)$, (after 750 time steps of size $\Delta t = 0.01$) for a shear flow with the following parameters: $\dot{\gamma} = 10$; $\lambda = 1$; $b = 150$; and $\eta_p = 1$. Figure 4 shows the transient behaviour of τ_{xx}, τ_{xy} and τ_{yy} over the time interval $t \in [0, 7.5]$. This plot matches Figure 2 in [11], which was obtained by solving the Fokker-Planck equation using a spectral element method, as well as a stochastic approach.

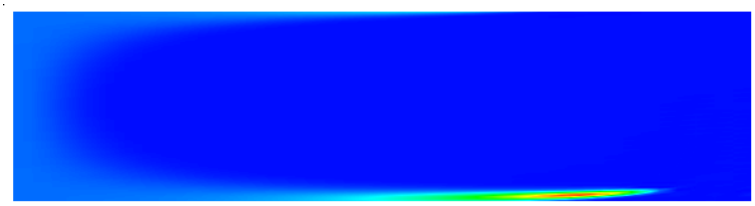

Figure 3: Steady state solution, $\alpha(\rho, \theta)$, of the Fokker-Planck equation for a 2D homogeneous shear flow. $\rho \in [0, \sqrt{b}]$ is on the horizontal axis, and $\theta \in [0, \pi]$ is on the vertical axis. The finite element mesh consisted of 20×40 quadrilateral elements, with quadratic basis functions.

The primary focus of this work is on simulating 3-dimensional flows. In order to solve the FP equation for the analogous 3D shear flow, we need to compute a large number of time steps on a highly refined 3-dimensional mesh. This is only feasible using parallel computation. We utilised libMesh's parallel computation facilities for this purpose, and solved the FP equation for 750 time steps with $\Delta t = 0.01$ for a mesh with $20 \times 80 \times 10$ hexahedral elements with tri-quadratic basis function on the Lonestar supercomputer at the Texas Advanced Computing Center. This machine contains 2560 processors and a peak performance of $\sim$ 6.7 TFlops. For the 3D shear flow computation shown in Figure 5 we used 40 processors. The load balancing for this computation is illustrated in Figure 6. The stress vs. time plot we obtained for the 3D flow is indistinguishable

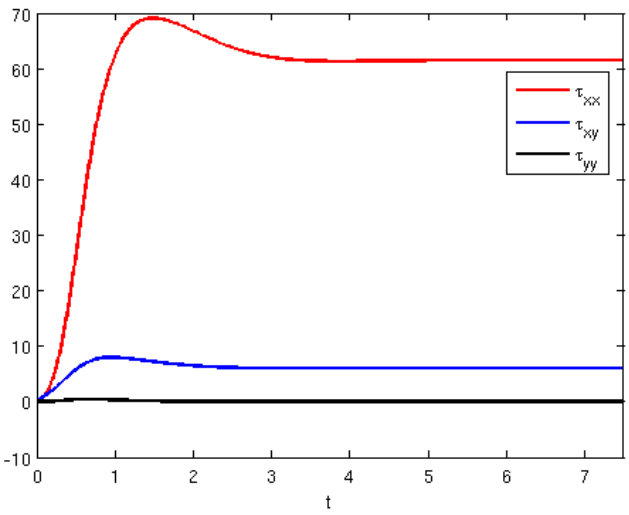

Figure 4: Stress vs. time for a 2D homogeneous shear flow.

to the 2D case shown in Figure 4. This precise agreement between the time dependent behaviour of the 2D and 3D FENE models in homogeneous shear flow agrees with the results in Section 4.2 of [25], in which it was suggested that the simpler 2D model is adequate for modelling this particular flow.

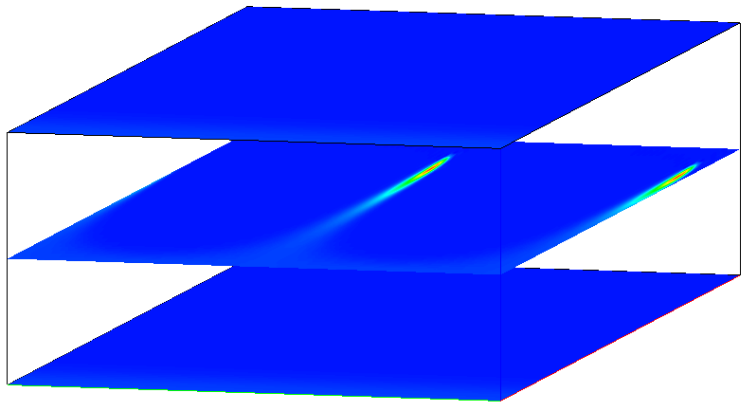

Figure 5: Cross sections of steady state solution, $\alpha(\rho, \theta, \varphi)$, of Fokker-Planck equation for a 3D homogeneous shear flow. The finite element mesh consisted of $20 \times 80 \times 10$ hexahedral elements with quadratic basis functions.

3.3 Extensional flows

Next we consider a homogeneous extensional flow. Again we begin with the 2-dimensional case, for which the velocity field is given by $\underset{\sim}{u} = (\dot{\varepsilon}x, -\dot{\varepsilon}y)$. Figure 7 shows the steady

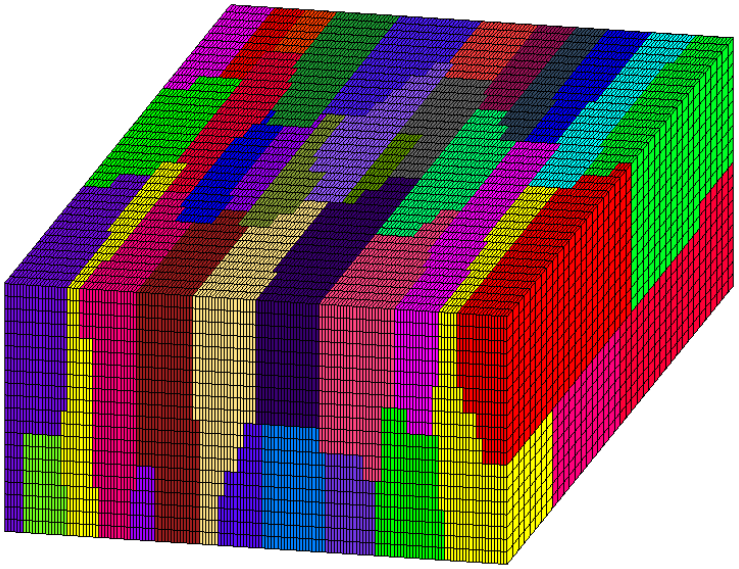

Figure 6: Load balancing for 3D shear flow. The mesh colouring reflects the partitioning of the domain into sub-domains handled by each of the 40 individual processors used in this computation.

state solution for a 2D extensional flow with $\dot{\varepsilon} = 1$, $\lambda = 1$, $b = 10$ and $\eta_p = 1$. Steady state was reached by time stepping to $t = 15$ with $\Delta t = 0.05$. For the FENE dumbbell model in extensional flow it is possible to derive the analytic solution of the FP equation and to determine $\underset{\approx}{\tau}$ exactly (see Section 13.5 of [7]). This is done for $\dot{\varepsilon} = 1$ in [11] in which τ_{xx} was given as: $\tau_{xx} = 9.37242277773$. Using our 25×25 mesh of quadratic elements, we computed the stress tensor $\underset{\approx}{\tau}$ over the interval $t \in [0, 15]$, shown in Figure 8, and our computed steady state value of τ_{xx} was correct to 5 significant digits.

Increasing the extension rate $\dot{\varepsilon}$ makes it more challenging to compute α. Figure 9 shows the solution of the Fokker–Planck equation with $\dot{\varepsilon} = 5$. The solution contains localised regions of very high gradients. It would be wasteful to compute this solution using a uniform mesh as the solution is benign throughout most of the domain. Therefore we have employed libMesh's adaptive mesh refinement capabilities. We used the magnitude of discontinuities in $\underset{\sim}{\nabla}_q \psi$ across element boundaries as a simple error indicator [19], and from Figure 9 one can see that the mesh has only been refined in the appropriate regions. Figure 10 shows the transient stress plot over $t \in [0, 15]$. Again, from [11] we have the exact steady state value of τ_{xx} for this flow, and our value of $\tau_{xx} = 122.21$, computed using the adaptively refined mesh, is correct to 4 significant digits.

Finally, we consider the case of a 3D homogeneous uniaxial extensional flow with

$$\underset{\approx}{\kappa} = \dot{\varepsilon} \begin{pmatrix} 1 & 0 & 0 \\ 0 & -0.5 & 0 \\ 0 & 0 & -0.5 \end{pmatrix}. \tag{3.2}$$

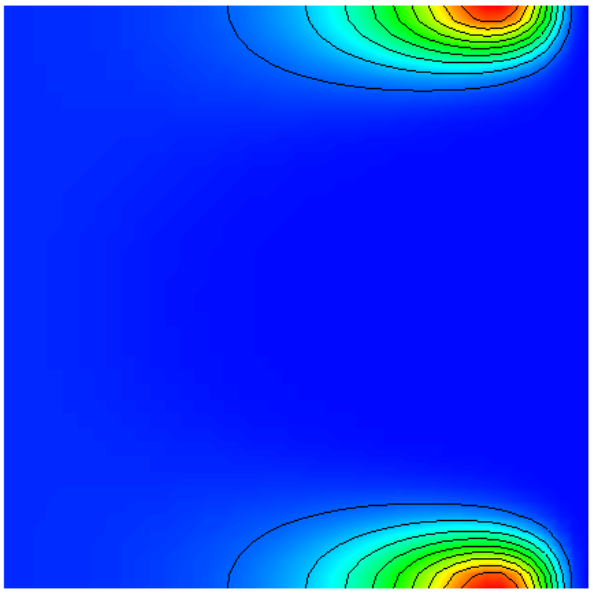

Figure 7: Steady state solution, $\alpha(\rho, \theta)$, of Fokker-Planck equation for a 2D homogeneous extensional flow with $\dot{\varepsilon} = 1$. $\rho \in [0, \sqrt{b}]$ is on the horizontal axis, and $\theta \in [0, \pi]$ is on the vertical axis. The finite element mesh consisted of 25×25 quadrilateral elements, with quadratic basis functions.

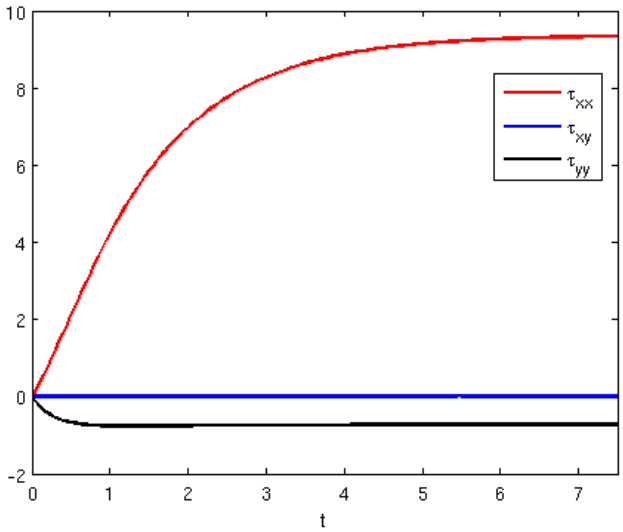

Figure 8: Stress vs. time for a 2D homogeneous extensional flow with $\dot{\varepsilon} = 1$.

Figure 11 shows the steady state solution for this velocity field, and Figure 12 is the accompanying transient stress plot for the 6 independent components of $\underset{\approx}{\tau}$.

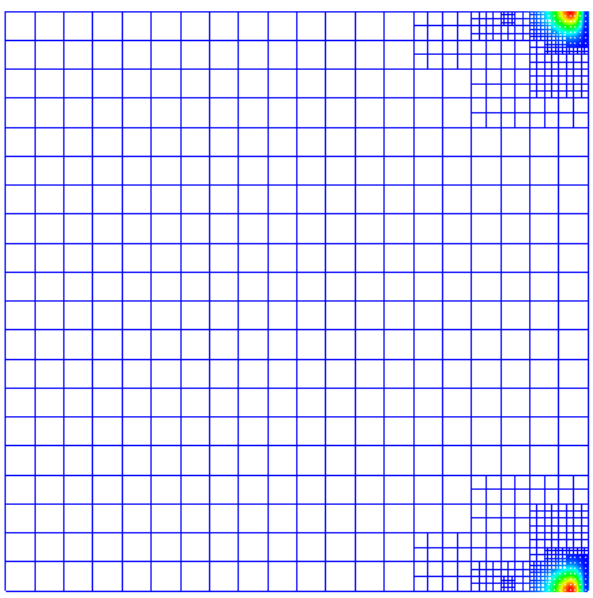

Figure 9: Steady state solution of Fokker-Planck equation for a 2D homogeneous extensional flow. Similar to Figure 7, except that here we have $\dot{\varepsilon} = 5$. We have plotted the adaptively refined mesh in this case, and one can see that refinement is focused on the regions of high gradients in the solution.

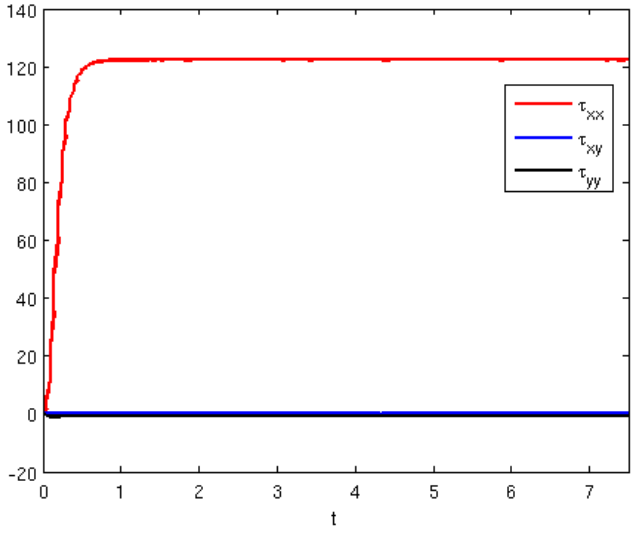

Figure 10: Stress vs. time for a 2D homogeneous extensional flow with $\dot{\varepsilon} = 5$.

3.4 Non-homogeneous flows

In this section we discuss the more challenging situation in which the velocity field $\underline{u}$ is allowed to vary through Ω. In contrast to the computations for homogeneous flows

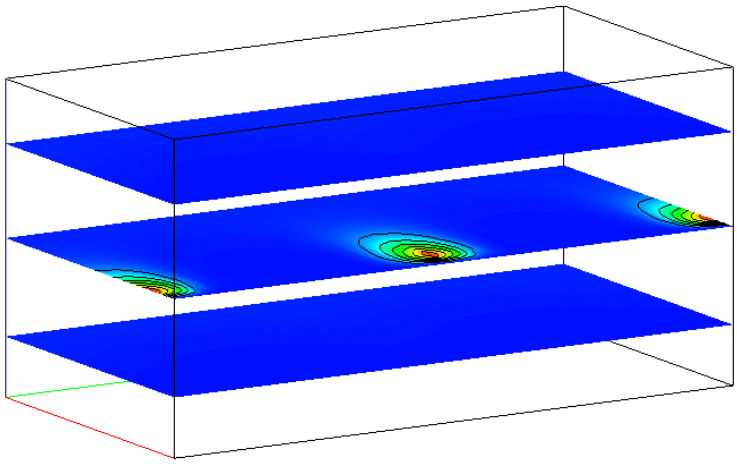

Figure 11: Steady state solution, $\alpha(\rho, \theta, \varphi)$, of Fokker-Planck equation for a 3D homogeneous uniaxial extensional flow. Mesh contained $30 \times 15 \times 15$ hexahedral elements with quadratic basis functions.

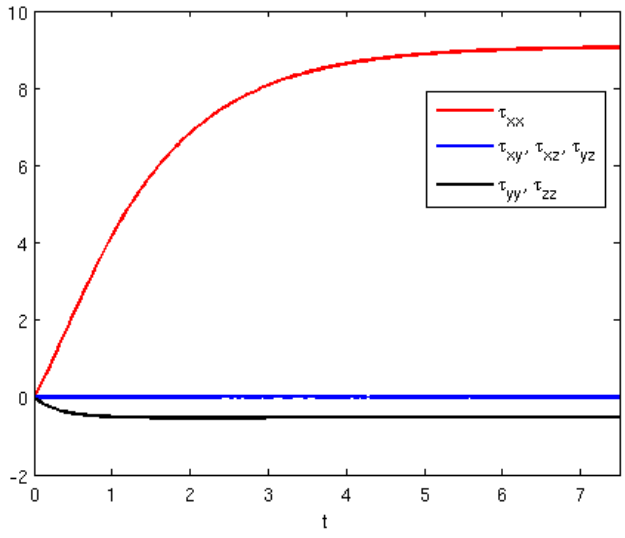

Figure 12: Stress vs. time for a 3D homogeneous uniaxial extensional flow. This plot looks qualitatively very similar to the stress plot for the 2D extensional flow in Figure 8. Though the plots are not identical, e.g. in the 2D case τ_{xx} converges to ~ 9.34, whereas in this 3D plot it converges to ~ 9.05.

considered in Section 3.1, we must now solve the full micro–macro problem using the procedure outlined in Section 2.3. We have applied our algorithm to a number of different flow geometries – one in 2D and one in 3D – for which results are presented below.

3.5 2-dimensional flow in a T-shaped domain

We consider a flow in a T-shaped domain in which both physical space and configuration space are assumed to be 2-dimensional. In this case, we have imposed periodic boundary conditions on the left-most and right-most edges of Ω, a rightward moving boundary at the top of the domain (such that $u_x = 1$ on that boundary), and a zero Dirichlet condition on the other boundaries. An alternative approach would be to impose velocities on inflow and outflow (e.g. a parabolic velocity profile), but the complication in this approach is that we do not have the solution to α upstream from the inflow boundary. The standard solution to this is to assume a fully developed flow upstream, for which α can be computed and convected into Ω. Nevertheless, we find it more convenient to use periodic boundary conditions, as the "upstream" solution is readily available by periodicity. As a result, we must drive the flow using moving walls. This means that this non-homogeneous flow is similar to a shear flow, and indeed in the main part of the channel we can see from Figure 15 that u_x is only slightly perturbed from a simple shear velocity profile. The simulation parameters in this case were $\lambda = 1, b = 10, \eta_p = 1.439$ and $\eta_s = 1$.

We ran this simulation on 8 processors, again on the Lonestar parallel computer at the Texas Advanced Computing Centre. We took 100 time steps with $\Delta t = 0.05$, in order to reach the steady state solution shown in the figures below. This computation took 81 seconds per time step, with 71% of the time for configuration space updates, and 23% for physical space updates. The physical space mesh consisted of 1024 bi-quadratic elements (4257 degrees of freedom), whereas the configuration space mesh had 400 bi-quadratic elements (1681 degrees of freedom). We have plotted (i) load balancing in physical and configuration space, (ii) configuration space and physical space cross sections of the steady state solution, α, (iii) components of the velocity field $\underset{\sim}{u}$ in $\partial\Omega$, and (iv) the components of $\underset{\approx}{\tau}$.

We have uniformly sized elements for our physical space mesh (element sizes shown in Figure 13). This necessitates a very fine mesh due to the singularities at the corners in the domain. It would be preferable to non-uniformly refine this mesh so that elements are larger away from the singularity – indeed it is likely that this would significantly reduce the computational work required to compute the solution to a given accuracy as for each degree of freedom we save in physical space, that is one less configuration space update we would require.

3.6 3-dimensional non-homogeneous flow

Finally, we consider a 3-dimensional non-homogeneous flow. The physical domain in this case is a rectangular prism (brick) and again we drive the flow using moving wall boundary conditions, and impose periodic boundary conditions on the ends of the brick. We have only one non-zero velocity component in this case, u_y, and our simulation parameters $(\lambda, b, \eta_s, \eta_p)$ are the same as in Section 3.5.

The configuration space mesh contained $10 \times 10 \times 10$ hexahedral elements with tensor-product quadratic basis functions, and the physical space mesh was quite coarse, con-

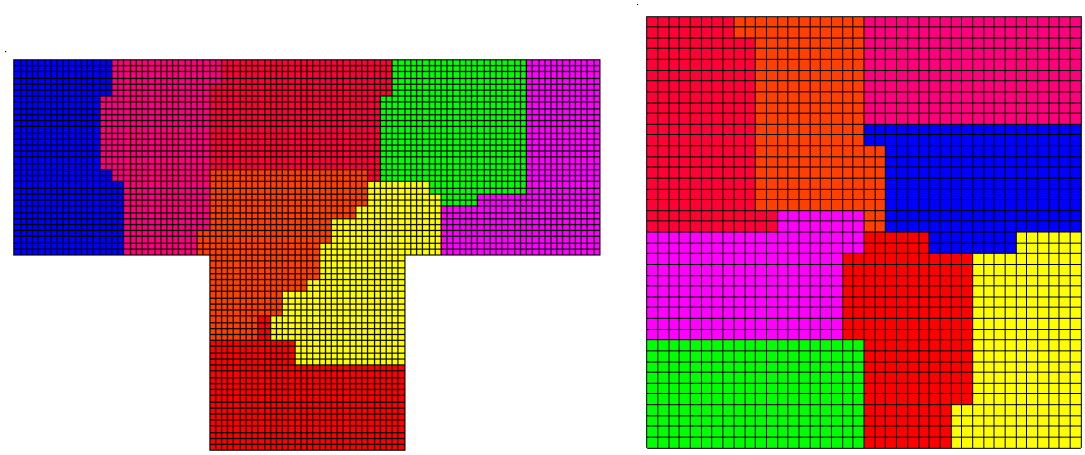

(a) (b)

Figure 13: Load balancing plots for computation in 2-dimensional T-domain. Computation was carried out on 8 processors. Figures (a) and (b) show mesh partitioning among the 8 processors for Ω and D respectively.

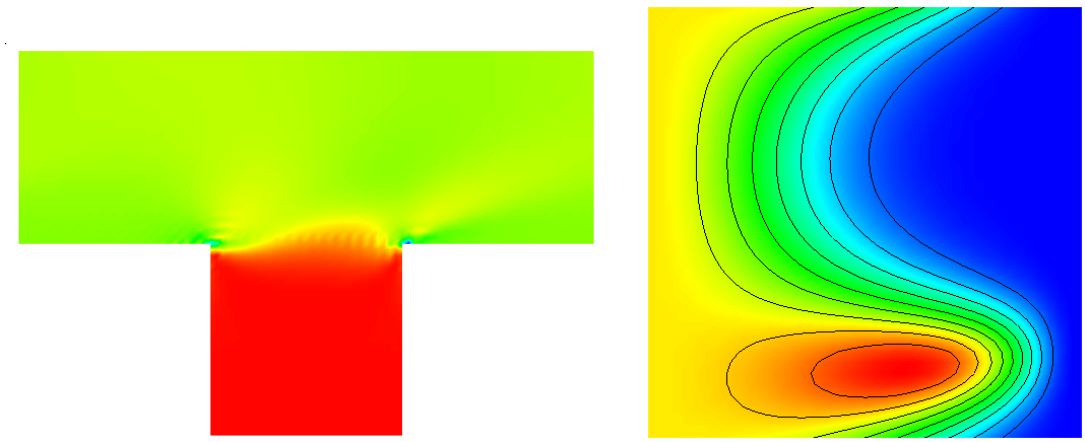

(a) (b)

Figure 14: Cross sections of α in (a) physical space and (b) configuration space.

taining only $4 \times 4 \times 4$ hexahedral elements. We ran the simulation for 60 time steps with $\Delta t = 0.05$ on the Lonestar supercomputer with 8 processors, and each time step took 129.9 seconds on average. The breakdown of computation time was similar to the 2D case: 74% of CPU time was spent on configuration space updates, and 20% was spent on physical space solves. We plot α, the velocity field and the components of the stress tensor in the figures below.

Fully 3D computations (i.e. 3D physical space and 3D configuration space) offer a major challenge. So far as we are aware, our work is the first attempt to use the deterministic method to perform a fully 3D simulation (Lozinski and Chauvière considered 3D

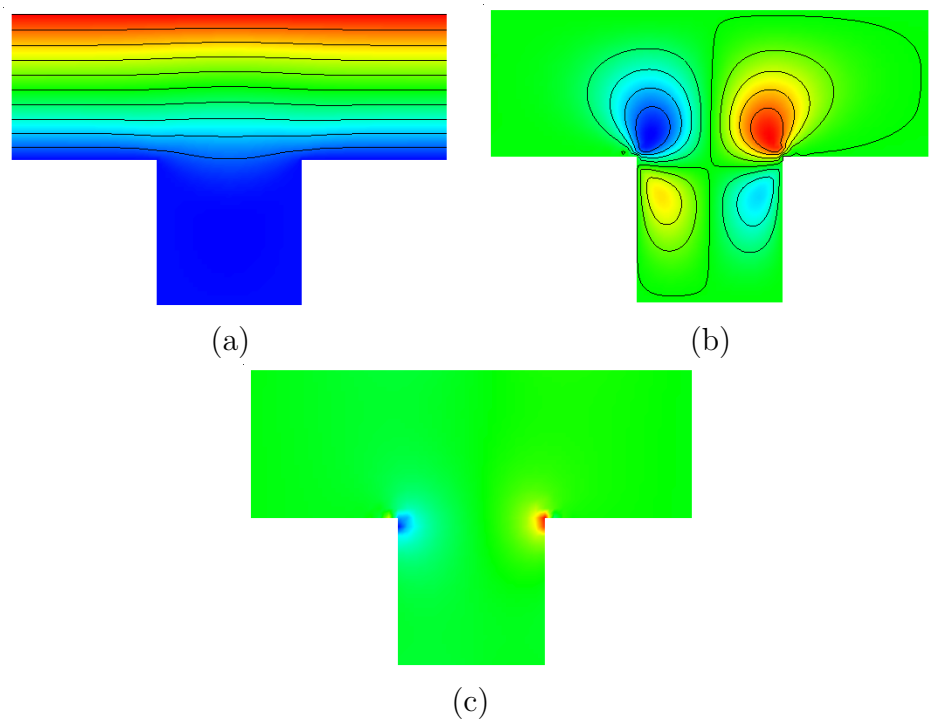

Figure 15: Steady state velocity and pressure profiles for T-domain computation. Figures (a) and (b) show u_x and u_y respectively. Note that u_x varies from 0 (blue) to 1 (red), and is only slightly perturbed from a uniform shear flow, whereas the range of u_y is only -0.03 (blue) to 0.03 (red). Figure (c) shows the pressure profile, and we can see the pressure singularity at the corners in the domain.

configuration space and 2D physical space in [10]). We intend to work toward simulating more complex 3-dimensional flows. Again, though, this will be a significant challenge. The primary difficulty we face is that as the number of degrees of freedom in the meshes increase, we require more sequential updates (both in configuration space and physical space). Increasing the number of processors used in the computation will at best keep the time for each update constant as the meshes are refined, but since we must perform more updates (possibly significantly more, as the number of degrees of freedom grows rapidly in 3D) then the overall CPU time for the computation will increase. We intend to investigate approaches to ameliorate this difficulty in our future work.

4 Future work and conclusions

There are a number of areas in which future work will be directed in order to further develop the ideas introduced in the preceding sections. These are outlined in this section.

As noted in Section 2, the bulk of the computational time in our deterministic micro-macro algorithm is spent in solving the configuration space part of the FP equation. Thus to improve the efficiency of our approach we would like to focus our attention on

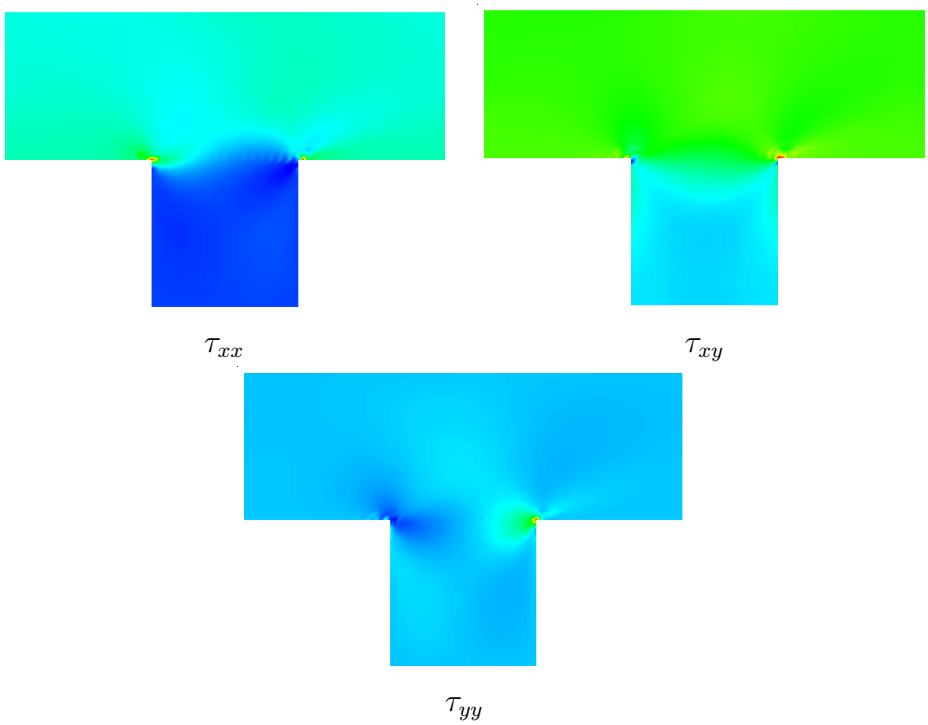

Figure 16: Components of $\underset{\approx}{\tau}$ for T-domain.

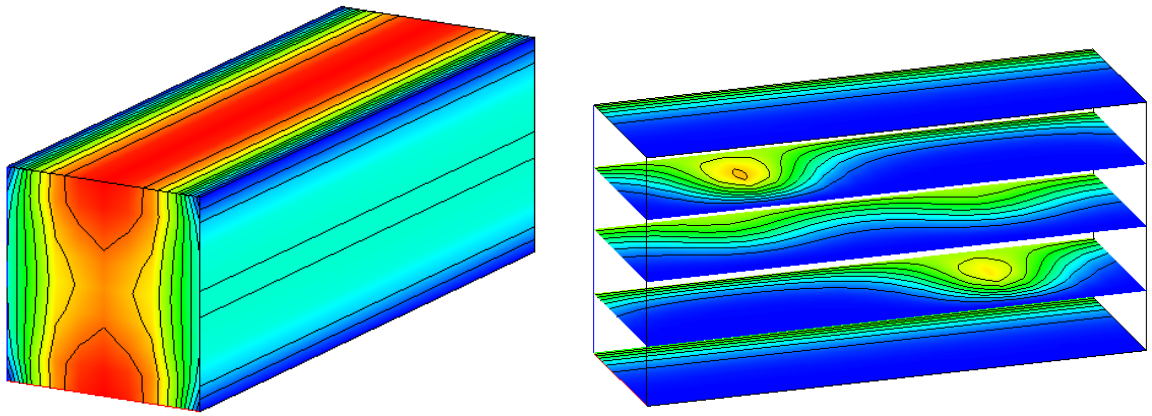

Figure 17: Cross sections of α in (a) physical space and (b) configuration space.

optimising this stage of the procedure. Following Süli [33], one approach to this would be to utilise stabilised sparse finite element methods. Approximation theory results for sparse finite element methods [9] show that they provide a way to obtain a certain level of accuracy with less degrees of freedom than for a full cartesian product mesh, although more stringent smoothness conditions are required. Also, the saving of degrees

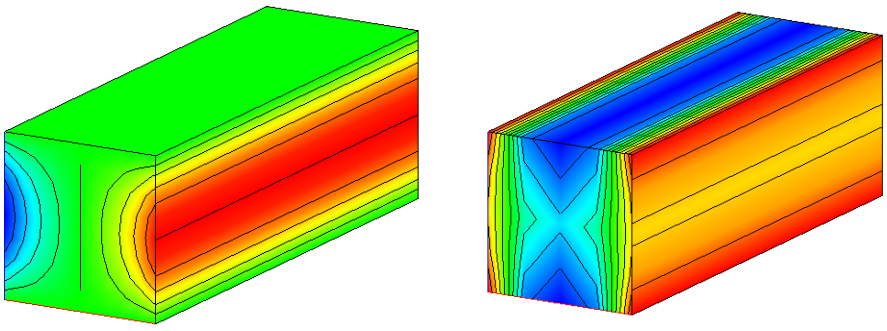

(a) (b)

Figure 18: Steady state velocity and pressure profiles for 3D domain. Figure (a) shows u_y. Note that u_x and u_z are identically zero for this flow and hence are not shown. Figure (b) shows the pressure profile.

of freedom becomes greater as the mesh dimensionality increases. If utilising sparse meshes enables us to reduce the number of degrees of freedom in configuration space, this could lead to significant savings as not only do we reduce the problem size for each configuration space update but we also reduce the number of physical space solves that need to be carried out.

Also, an important open question is whether it is feasible to utilise a deterministic approach for models in which the configuration space is of dimensionality greater than 3, such as those arising from the Rouse-Zimm chain polymer model. We suggest that sparse meshes may make this viable. Indeed, in [13], computations were carried out using this approach for a simple homogeneous shear flow with configuration space of dimensionality up to 6. From the reported results, the sparse mesh approach appears to offer significant improvement in efficiency compared to using a full tensor product mesh. Applying a sparse mesh method to bead-spring chain models, especially for non-homogeneous flows, is an interesting topic that we would like to explore in future work.

To date, we have focused primarily on the practicalities of implementing our deterministic micro-macro algorithm from Section 2, and testing this algorithm by simulating various flows. An important direction for future research is to refine the mathematical analysis of our algorithm. One point requiring clarification is the choice of function spaces for the weak formulation of the FP equation after operator-splitting. We referred to the function spaces as K and M in Section 2, but did not specify anything about the structure of these spaces. Also, we would like to consider the question of convergence of the deterministic algorithm. In the work of Lozinski *et. al.* (e.g. [10, 11, 26]), convergence is demonstrated empirically for their deterministic approach by showing that the solution converges with mesh refinement. We would like to address this more rigorously.

The FP equation in physical space is a linear transport equation. It appears that the Galerkin approach to solving this equation works well for simple flows, but may break down for more complex velocity fields. We would like to investigate this further,

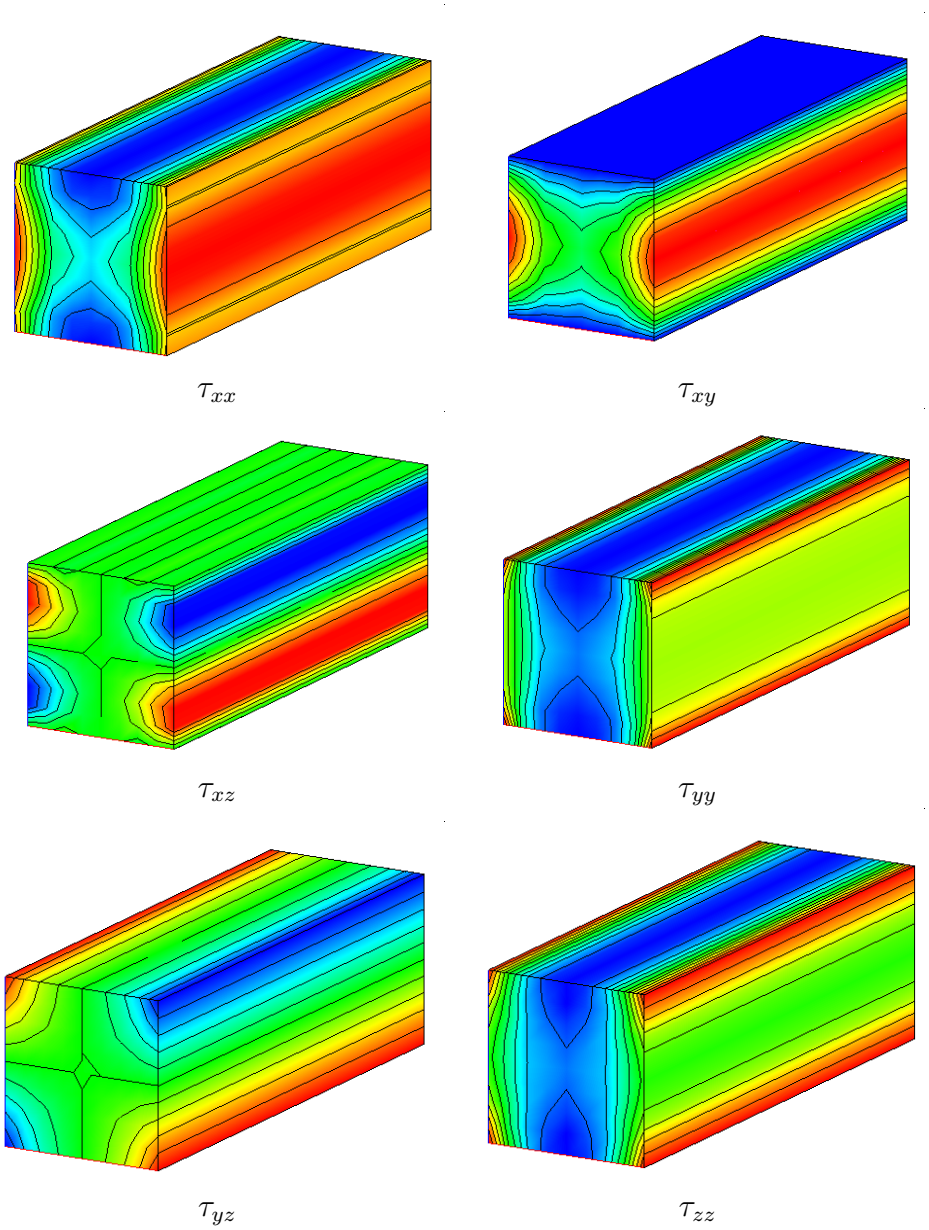

Figure 19: Independent components of the polymeric extra stress tensor, $\underset{\approx}{\tau}$ for the 3D domain.

and perhaps use a stabilised method, such as SUPG, to improve the robustness of our methodology when applying it to complex flows.

We would also like to analyse the impact that the accuracy of $\psi(\underset{\sim}{x}, \cdot, t)$ has on the macroscopic quantities of interest, $\underset{\approx}{\tau}(\underset{\sim}{x}, t)$ and $\underset{\sim}{u}(\underset{\sim}{x}, t)$. Since we average ψ in order to compute $\underset{\approx}{\tau}$ it seems likely that the accuracy of ψ is not as critical as we may have assumed. If we have a rigorous description of the relationship between the microscopic and macroscopic variables, it could enable us to allocate computational resources more efficiently.

We have examined a finite element based methodology for computing solutions of the multiscale Navier–Stokes Fokker–Planck model that describes the dynamics of dilute polymeric fluids. In Section 1 we discussed the physical and mathematical foundations of the NS–FP model, and in Section 2 we presented a review of the literature on computational simulation of polymeric fluids, and then discussed our deterministic algorithm in detail. We presented a range of numerical results in Section 3 that demonstrated the effectiveness of our approach, including some novel results for the simulation of a fully 3-dimensional flow. Nevertheless, there remains much work to be done in refining the deterministic approach examined in this work. In pursuing the directions of future work briefly discussed above, we intend to push the limits of the deterministic approach to see if it can compete with well developed stochastic approaches in simulating a wide range of polymeric flows.

Acknowledgements
I am very grateful to my D.Phil. supervisor, Professor Endre Süli, for his help and guidance in this work.

References

[1] Barrett, J., Schwab, C., and Süli, E. Existence of global weak solutions for some polymeric flow models. *Math. Models and Methods in Applied Sciences 15*, 3 (2005), 939–983.

[2] Barrett, J., and Süli, E. Existence of global weak solutions to kinetic models of dilute polymers. *Oxford University Computing Laboratory, NA-06/14* (2006).

[3] Batchelor, G. *An introduction to fluid dynamics*. Cambridge University Press, 1967.

[4] Bhave, A., Armstrong, R., and Brown, R. Kinetic theory and rheology of dilute, nonhomogeneous polymer structures. *J. Chem. Phys. 95* (1991), 2988–3000.

[5] Biller, P., and Petruccione, F. The flow of dilute polymer solutions in confined geometries: a consistent numerical approach. *J. Non-Newtonian Fluid Mech. 25* (1987), 347–364.

[6] Bird, R., Curtiss, C., Armstrong, R., and Hassager, O. *Dynamics of Polymeric Liquids, Volume 1, Fluid Mechanics*, second ed. John Wiley and Sons, 1987.

[7] Bird, R., Curtiss, C., Armstrong, R., and Hassager, O. *Dynamics of Polymeric Liquids, Volume 2, Kinetic Theory*, second ed. John Wiley and Sons, 1987.

[8] Brenner, S., and Scott, L. *The Mathematical Theory of Finite Element Methods*, second ed. Springer, 2002.

[9] Bungartz, H., and Griebel, M. Sparse grids. *Acta Numerica* (2004), 1–123.

[10] Chauvière, C., and Lozinski, A. Simulation of complex viscoelastic flows using Fokker-Planck equation: 3D FENE model. *J. Non-Newtonian Fluid Mech. 122* (2004), 201–214.

[11] Chauvière, C., and Lozinski, A. Simulation of dilute polymer solutions using a Fokker-Planck equation. *Computers and Fluids 33* (2004), 687–696.

[12] Chauvière, C., and Owens, R. A new spectral element method for the reliable computation of viscoelastic flow. *Comput. Methods Appl. Mech. Eng. 190* (2001), 3999–4018.

[13] Delaunay, P., Lozinski, A., and Owens, R. Sparse tensor-product Fokker-Planck-based methods for nonlinear bead-spring chain models of dilute polymer solutions. *CRM Proceedings and Lecture Notes* (2006). preprint.

[14] Fan, X. Viscosity, first normal stress coefficient and molecular stretching in dilute polymer solutions. *J. Non-Newtonian Fluid Mech. 17* (1985), 125–144.

[15] Fan, X. Molecular models and flow calculations: Ii. simulation of steady planar flow. *Acta Mechanica Sinica 5* (1989), 216–226.

[16] Grosso, M., Maffettone, P., Halin, P., Keunings, R., and Legat, V. Flow of nematic polymers in eccentric cylinder geometry: influence of closure approximations. *J. Non-Newtonian Fluid Mech. 94* (2000), 119–134.

[17] Halin, P., Lielens, G., Keunings, R., and Legat, V. The lagranian particle method for macroscopic and micro-macro viscoelastic flow computations. *J. Non-Newtonian Fluid Mech. 79* (1998), 387–403.

[18] Hulsen, M., van Heel, A., and van den Brule, B. Simulation of viscoelastic flows using brownian configuration fields. *J. Non-Newtonian Fluid Mech. 70* (1997), 79–101.

[19] Kelly, D., Gago, J., Zienkiewicz, O., and Babuška, I. A posteriori error analysis and adaptive processes in the finite element method: Part i error analysis. *International Journal for Numerical Methods in Engineering 19* (1981), 1593–1619.

[20] Keunings, R. A survey of computational rheology. In *XIIIth international congress on rheology* (Cambridge, UK, August 2000). Available at `http://www.mate.tue.nl/~hulsen`.

[21] Keunings, R. Micro–macro methods for the multiscale simulation of viscoelastic flow using molecular models of kinetic theory. *Rheology Review* (2004), 67–98.

[22] Kirk, B., Peterson, J., Stogner, R., and G.F., C. libmesh: A c++ library for parallel adaptive mesh refinement/coarsening simulations. *Engineering with Computers* (2006). in review.

[23] Kramers, H. The viscosity of macromolecules in a streaming fluid. *Physica 11*, 1 (1944).

[24] Laso, M., and Öttinger, H. Calculation of viscoelatic flow using molecular models: the connffessit approach. vol. 47, pp. 1–20.

[25] Lozinski, A. *Spectral methods for kinetic theory models of viscoelastic fluids*. PhD thesis, École Polytechnique Fédérale de Lausanne, 2003.

[26] Lozinski, A., and Chauvière. A fast solver for Fokker-Planck equation applied to viscoelastic flows calculation: 2D FENE model. *Journal of Computational Physics 189* (2003), 607–625.

[27] Lozinski, A., Chauvière, C., Fang, J., and Owens, R. Fokker-Planck simulations of fast flows of melts and concentrated polymer solutions in complex geometries. *J. Rheology 47* (2003), 535–561.

[28] Nayak, R. *Molecular simulation of liquid crystal polymer flow: a wavelet-finite element analysis*. PhD thesis, MIT, 1998.

[29] Oldroyd, J. On the formulation of rheological equations of state. *Proc. Roy. Soc. London* (1950), 523–541.

[30] Öttinger, H. *Stochastic processes in polymeric fluids*. Springer, 1996.

[31] Rouse, P. A theory of the linear viscoelastic properties of dilute soluns of coiling polymers. *J. Chem. Phys. 21* (1953), 1272–1280.

[32] Stewart, W., and Sørensen, J. Hydrodynamic interaction effects in rigid dumbbell suspensions. ii. computations for steady shear flow. *Trans. Soc. Rheol. 16* (1972), 1–13.

[33] Süli, E. Finite element approximation of high-dimensional transport-dominated diffusion problems. *Oxford University Computing Laboratory, NA-05/19* (2005).

[34] Warner, H. Kinetic theory and rheology of dilute suspensions of finitely extendible dumbbells. *Ind. Eng. Chem. Fundamentals* (1972), 379–387.

[35] Zimm, B. Dynamics of polymer molecules in dilute solution: viscoelasticity, flow birefringence and dielectric loss. *J. Chem. Phys. 24* (1956), 269–278.